2011

Assessment of exposure to composite nanomaterials and development of a personal respiratory deposition sampler for nanoparticles

Lorenzo Cena
University of Iowa

ASSESSMENT OF EXPOSURE TO COMPOSITE NANOMATERIALS AND DEVELOPMENT OF A PERSONAL RESPIRATORY DEPOSITION SAMPLER FOR NANOPARTICLES

by

Lorenzo Cena

An Abstract

Of a thesis submitted in partial fulfillment
of the requirements for the Doctor of Philosophy degree in
Occupational and Environmental Health (Industrial Hygiene)
in the Graduate College of
The University of Iowa

May 2011

Thesis Supervisor: Associate Professor Thomas M. Peters

ABSTRACT

The overall goals of this doctoral dissertation are to provide knowledge of workers' exposure to nanomaterials and to assist in the development of standard methods to measure personal exposure to nanomaterials in workplace environments.

To achieve the first goal, a field study investigated airborne particles generated from the weighing of bulk carbon nanotubes (CNTs) and the manual sanding of epoxy test samples reinforced with CNTs. This study also evaluated the effectiveness of three local exhaust ventilation (LEV) conditions (no LEV, custom fume hood and biosafety cabinet) for control of exposure to particles generated during sanding of CNT-epoxy nanocomposites. Particle number and respirable mass concentrations were measured with direct-read instruments, and particle morphology was determined by electron microscopy. Sanding of CNT-epoxy nanocomposites released respirable size airborne particles with protruding CNTs very different in morphology from bulk CNTs that tended to remain in clusters (>1μm). Respirable mass concentrations in the operator's breathing zone were significantly greater when sanding took place in the custom hood ($p < 0.0001$) compared to the other LEV conditions. This study found that workers' exposure was to particles containing protruding CNTs rather than to bulk CNT particles. Particular attention should be placed in the design and selection of hoods to minimize exposure.

Two laboratory studies were conducted to realize the second goal. Collection efficiency of submicrometer particles was evaluated for nylon mesh screens with three pore sizes (60, 100 and 180 μm) at three flow rates (2.5, 4, and 6 Lpm). Single-fiber efficiency of nylon mesh screens was then calculated and compared to a theoretical estimation expression. The effects of particle morphology on collection efficiency were also experimentally measured. The collection efficiency of the screens was found to vary by less than 4% regardless of particle morphology. Single-fiber efficiency of the screens calculated from experimental data was in good agreement with that estimated from theory

for particles between 40 and 150 nm but deviated from theory for particles outside of this range. New coefficients for the single-fiber efficiency model were identified that minimized the sum of square error (SSE) between the experimental values and those estimated with the model. Compared to the original theory, the SSE calculated using the modified theory was at least threefold lower for all screens and flow rates. Since nylon fibers produce no significant spectral interference when ashed for spectrometric examination, the ability to accurately estimate collection efficiency of submicrometer particles makes nylon mesh screens an attractive collection substrate for nanoparticles.

In the third study, laboratory experiments were conducted to develop a novel nanoparticle respiratory deposition (NRD) sampler that selectively collects nanoparticles in a worker's breathing zone apart from larger particles. The NRD sampler consists of a respirable cyclone fitted with an impactor and a diffusion stage containing eight nylon-mesh screens. A sampling criterion for nano-particulate matter (NPM) was developed and set as the target for the collection efficiency of the NRD sampler. The sampler operates at 2.5 Lpm and fits on a worker's lapel. The cut-off diameter of the impactor was experimentally measured to be 300 nm with a sharpness of 1.53. Loading at typical workplace levels was found to have no significant effect (2-way ANOVA, $p=0.257$) on the performance of the impactor. The effective deposition of particles onto the diffusion stage was found to match the NPM criterion, showing that a sample collected with the NRD sampler represents the concentration of nanoparticles deposited in the human respiratory system.

Abstract Approved: _____
Thesis Supervisor

_____
Title and Department

_____
Date

ASSESSMENT OF EXPOSURE TO COMPOSITE NANOMATERIALS AND DEVELOPMENT OF A PERSONAL RESPIRATORY DEPOSITION SAMPLER FOR NANOPARTICLES

by

Lorenzo Cena

A thesis submitted in partial fulfillment
of the requirements for the Doctor of Philosophy degree in
Occupational and Environmental Health (Industrial Hygiene)
in the Graduate College of
The University of Iowa

May 2011

Thesis Supervisor: Associate Professor Thomas M. Peters

Graduate College
The University of Iowa
Iowa City, Iowa

CERTIFICATE OF APPROVAL

_____

PH.D. THESIS

_____

This is to certify that the Ph. D. thesis of

Lorenzo Cena

has been approved by the Examining Committee for the thesis requirement for the Doctor of Philosophy degree in Occupational and Environmental Health (Industrial Hygiene) at the May 2011 graduation.

Thesis Committee: _____
Thomas Peters, Thesis Supervisor

_____
Patrick O'Shaughnessy

_____
Renée Anthony

_____
Vicki Grassian

_____
Jacob Oleson

To Ashley, Sofia and Liliana

This know also, that in the last days perilous times shall come. For men shall be [...] ever learning, and never able to come to the knowledge of the truth.

II Timothy 3:1-2,7

ACKNOWLEDGMENTS

I wish to show my gratitude first and foremost to God, for blessing me with opportunities throughout my life that have led me to the achievement of my Ph.D., one of the highest levels of education. My parents taught me the importance of obtaining an education and showed me how hard work, sacrifice and integrity lead to achieving great things in life. My wife Ashley, my beloved eternal companion, has supported me in every step, has encouraged me when I was down, has shared with me every joy and gloom and has patiently endured with me many years of student life. My two daughters Sofia and Liliana have greeted me with shouts of joy, hugs and kisses every night when I arrived home and have made every day worth living.

I owe deep gratitude to my advisor, Tom Peters, who has not only taught me everything I know about aerosols, but has also spent countless hours helping me improve my writing and presentation skills. My committee members, Renée Anthony, Patrick O'Shaughnessy, Vicki Grassian and Jacob Oleson, with their expertise have taught me how to design experiments, set and test criteria for success, and improve my research.

I would also like to thank Eric Sawvel, Donna Vosburgh, Mike Humann, Will Cyrs, and Kerry Krause, fellow students who have worked with me on class projects and lab experiments. Dr. Bon Ki Ku, Betsy Shelton, Janet Watt and my brother Fabrizio assisted me in the collection of data. Dr. Maura Sheehan has mentored and encouraged me. Doug Dowis of SKC, Inc. first introduced me to industrial hygiene equipment and placed in me the initial aerosol spark. Del Bonney has helped me with my writing. The University of Iowa Central Microscopy research facilities and RJ Lee Group of Monroeville, PA have provided assistance with the scanning and transmission electron microscopes.

This research was supported by a Heartland Center for Occupational Health and Safety pilot project grant (T42OH008491) and NIOSH KO1 award (OH009255).

TABLE OF CONTENTS

LIST OF TABLES

LIST OF FIGURES

CHAPTER I

INTRODUCTION

Nanoparticles in the Workplace

Nanoparticles are particles with at least one external dimension smaller than 100 nm (ASTM, 2006) that can originate from a variety of occupational sources. Hot background processes, such as engine combustion, arc welding and the burning of natural gas, produce vaporized materials. As these vapors cool, they nucleate to form incidental nanoparticles (Hinds, 1999). In contrast, some particles in the workplace are engineered. Materials with nano-scale features exhibit unusual physical, chemical and biological properties that can enhance consumer products (Nel et al., 2006). Consequently, these bulk, engineered nanoparticles can be incorporated in matrix structures to form nanocomposite materials. Many products containing engineered nanoparticles are commercially available (Hansen et al., 2008). The nanotechnology industry has been projected to employ millions of workers worldwide within the next decade (Roco, 2004), which will entail the exposure of a large population of workers to new materials for which little is known about their toxicity (Schulte et al., 2008a).

Exposure to nanoparticles may occur in a variety of workplace settings, including research laboratories, production manufacturing facilities, and waste handling systems (Schulte et al., 2008b). Studies have been conducted to evaluate occupational exposure to incidental nanoparticles; however, few studies have focused on the exposure to engineered nanoparticles (Stern and McNeil, 2008). Kuhlbusch et al. (2004) measured aerosol concentrations in three carbon black production facilities and found relatively small increases in nanoparticle number concentrations compared to background measurements. These increases were attributed to background sources such as forklift and gas heater emissions. In an occupational exposure study in an engine machining facility, Peters et al. (2006) found that high background incidental nanoparticle levels from direct-

fire, natural gas furnace exhaust often exceeded those produced by the machining processes. Elihn and Berg (2009) measured and characterized ultrafine particles in seven industrial plants, finding elevated particle number concentrations during aluminum fettling processes, laser cutting, welding, and smelting. They concluded that the quality of the ventilation, the use of local exhaust ventilation and the use of forklift trucks played an important role in number concentration levels of ultrafines.

Exposure to engineered nanoparticles can occur throughout a product's lifecycle (Stern and McNeil, 2008). As these nanoparticles are incorporated in consumer products, exposures can take place during manufacturing, use, disposal and recycling of consumer products. Methner et al. (2007) evaluated exposure to carbon nanofibers (CNF) during chopping, transferring and mechanically mixing of the nanofibers, as well as cutting CNF-composite material using a table saw. They found slight increases in airborne concentrations (number and mass) during transferring, mixing and cutting, indicating that the potential for release of engineered nanomaterials does exist during these processes. In contrast, others have found that handling of nanomaterials in manufacturing facilities generates exposures to larger (>200 nm) nanoparticle agglomerates (Peters et al., 2009a; Evans et al., 2010).

There are several commercially available air sampling instruments that can characterize exposure to nano-scale aerosols; however, none are small enough to be worn by workers and allow estimation of nanoparticle concentration in the breathing zone (Methner et al., 2010a). To overcome this limitation, attempts have been made to use a variety of instruments to characterize nano-scale aerosols. Park et al. (2010) measured incidental nanoparticles concentrations in three workplace environments using a combination of aerosol photometers for mass concentrations, a scanning mobility particle sizer for size distributions, a surface area monitor and an optical particle counter for number concentrations. The instruments were placed on a cart and a mannequin was used as reference for the location of the sampling tubes at breathing zone heights. The results

showed that surface area and fine particle number were more sensitive measures of spatial variation of nanoparticles than mass concentrations, however, the authors recommended a multi-metric sampling approach for nanoparticle exposure assessment.

Similarly, Methner et al. (2010a and 2010b) combined two direct-read instruments (a concentration particle counter and an optical particle counter), which were supplemented by two filter-based air samplers. Filter samples were used to differentiate between incidental and engineered nanoparticles (through electron microscopy and chemical analysis), which could not be made with the direct-read instruments alone. The use of a combination of direct-read instruments and the addition of filter samples is useful for characterizing release of nanomaterials in the workplace; however, the use of costly equipment and the generation of large amount of data requiring complicated analytical techniques limit their use by exposure assessors such as industrial hygienists. Direct-read instruments are discussed in more details in the Direct-read Instruments, Area Samplers and Their Limitations section.

Toxicity of Nanoparticles

Some engineered nanoparticles have been shown to exert greater toxic response than larger particles of the same composition (Papp et al., 2008). Several groups have identified that, for a given mass dose of titanium dioxide (TiO_2), a poorly soluble, low-toxicity material, pulmonary inflammatory response and tissue damage is greater if the dose is composed of nano-sized particles rather than larger particles (Oberdörster et al., 1994; Duffin et al., 2007). However, additional factors affect toxicity of nanoparticles, including the physical and chemical reactivity and activity of individual particles that compose the material (Grassian et al., 2007; Grassian, 2008; Jiang et al., 2008; Bastian et al., 2009) and the surface charge and agglomeration state of a nanoparticle (Jiang et al., 2009).

Compared to larger particles, copper oxide nanoparticles were found to be more cytotoxic and genotoxic and showed much higher ability to cause mitochondrial depolarization and oxidative DNA damage (Karlsson et al., 2009). Others have identified similar behavior for copper nanoparticles (Chen et al., 2006; Grassian et al., 2007). Further, the work of Karlsson et al. (2009) showed that iron oxide particles exerted low toxicity, while TiO_2 nanoparticles were shown to have relatively high ability to damage DNA. Cha et al. (2008) found that silver nanoparticles induced a greater degree of inflammation in rodent livers (*in vivo* exposures) and a greater degree of apoptosis in human liver cells (*in vitro*) when compared to micrometer-sized silver particles. Chen et al. (2006) identified that copper nanoparticles exerted toxic effects on rodent kidney, liver and spleen, whereas micrometer-sized copper did not show the same pathological effects and tissue damage. Instillation of carbon black nanoparticles (500 μg), TiO_2 nanoparticles (125 μg) and latex nanoparticles (125 μg) into rat lungs were all found capable of causing more airway inflammation than larger particles of the same composition (Donaldson et al., 2000).

Exposure to incidental nanoparticles has been associated with adverse health outcomes in occupational settings. Acute respiratory distress syndrome triggered by exposure to metal nanoparticles was suspected as the cause of severe illness and death of several nickel smelters (Sandstrom et al., 1989). No exposure levels were reported for these workers. Respiratory distress syndrome was also identified as the cause of death of a worker who inhaled one gram of nickel nanoparticles over a 90-minute period while spraying nickel using a thermal arc process (Rendall et al., 1994; Phillips et al., 2010). Exposure to annual average nanoparticle concentrations above 13,000 particles/cm^3 has been associated with increased asthma symptoms (Wichmann et al., 2000). Additionally, exposure to welding fume (average $PM_{2.5}$ concentrations = 0.7 ± 0.8 mg/m^3) has been associated with adverse alterations in cardiac autonomic function (Magari et al., 2001). Numerous studies have related exposure to incidental nanoparticles with increased risk of

hospital admission for heart attack (average concentrations > 12,500 particles/cm^3, von Klot et al., 2005), changes in cardiac autonomic function (average concentrations > 17,000 particles/cm^3, Timonen et al., 2005) and increased prevalence of asthma (average concentrations > 13,000 particles/cm^3, Lwebuga-Mukasa et al., 2005). The lack of standard methods to assess personal exposure to nanoparticles, however, has severely limited the epidemiologic tie between exposure and adverse health outcomes.

Carbon Nanotubes

Characterization of exposure to carbon nanotubes (CNTs) is the topic of Chapter II of this dissertation; therefore, special focus on CNT literature will be given in this section. CNTs are commonly used because they have exceptional physical and chemical properties. The International Organization for Standardization (ISO) defines particles with two external dimensions smaller than 100 nm as nanofibers or, if hollow, nanotubes (ISO, 2008). Carbon nanotubes were first discovered in 1991 and consist of single or multiple layers of graphene wrapped into a cylindrical structure (Iijima, 1991). Their unusual properties (e.g. increased electrical and thermal properties, tensile strength) make them a desirable material for industrial and commercial applications (Yu et al., 2000; Lau & Hui, 2002). There are several forms of CNTs (single-walled, multi-walled, with or without residual metal catalysts, surface coated, long, short, etc.) commercially available and used in many applications such as electronics, lithium-ion batteries, solar cells, super capacitors, reinforced plastics, micro-fabrication conjugated polymer activators, biosensors, and biomedical devices (NIOSH, 2010).

Worker exposures to CNTs are poorly characterized. There are only a handful of studies reporting workplace exposure measurements, but these studies confirm that exposure to CNTs may vary greatly depending on the process and the type of engineering controls used such as ventilated enclosures (NIOSH, 2010). Bello et al. (2008) found no increase in total particle number concentration during production and handling of CNTs

compared to background measurements when operating a CNT growth furnace and removing the CNTs after furnace cool-down. Mechanical agitation, however, may produce significantly higher concentrations. Han et al. (2008) measured concentrations in a CNT manufacturing laboratory ranging from 37 $\mu g/m^3$ during weighing operations to 430 $\mu g/m^3$ during blending operations with no controls in place, while concentrations were lowered below the limit of detection once the weighing and blending processes took place in a ventilated enclosure. Similar elevated concentrations during agitation of CNTs were measured by Maynard et al. (2004), ranging from 0.7 to 53 $\mu g/m^3$ with no engineering controls in place, and by Johnson et al. (2010), who found significantly higher number concentrations during sonication of water-CNT solutions than during weighing and transferring of dry CNTs. Aerosolized CNTs were also observed to remain in agglomerated bundles larger than 1 μm (Maynard et al., 2004).

The effects of engineering controls were observed in the work of Lee et al. (2010) and Tsai et al. (2009a). Measurements taken in seven industrial or laboratory facilities by Lee et al. (2010) indicated that preparation and ultrasonic dispersion of CNTs inside a laboratory fume hood generated the release of metal particles used as catalysts during CNT synthesis. No detectable amounts of CNTs were found on filter samples collected during the CNT synthesis and handling processes (Lee et al., 2010). In a CNT production laboratory, Tsai et al. (2009a) found that particle number concentrations measured during CNT synthesis inside a chemical fume hood were elevated (ranging between 10^7 and 4×10^6 particles/cm^3), while concentrations measured in samples placed at breathing zone height outside the hood were similar to background concentration measurements. No operator was present at the hood face during the process and measurements, thus avoiding the generation of turbulent flows at the hood's face (Kim and Flynn, 1991). These flows have been found to cause a more extensive release of nanoparticles and exposure of workers during handling of nanopowders due to the formation of complex airflow patterns between the worker and the hood (Tsai et al., 2009b).

CNTs in finished products are often embedded in polymer matrices; however, little information exists in the literature about exposure to these matrix-embedded CNT nanocomposites during mechanical processing of finished products. Bello et al. (2009) investigated the release of particles during simulations of industrial wet and dry cutting of CNT-composite materials and found substantial increases in mass-based aerosol concentrations during dry cutting compared to background measurements. Characterization of exposure to these embedded CNTs is necessary to determine whether the exposure originates from the polymer matrix holding the CNTs, from CNTs that break off during the mechanical processing and become airborne or a combination of the two.

Several toxicological studies have linked exposure to CNTs with adverse health effects. Current studies on CNT exposure are based on animal exposure data. These studies have shown adverse lung effects such as pulmonary inflammation, granulomas, fibrosis and diminished resistance to pathogenic attacks (Wareith et al., 2003; Muller et al., 2005; Shvedova et al., 2005 and 2008; Lam et al., 2006; Porter et al., 2010; Pauluhn, 2010). Similarly to asbestos fibers, CNTs have been observed to migrate from the lungs to other organs (Hubbs et al., 2009; Porter et al., 2010; Mercer et al., 2010). Adverse cardiac health effects, such as oxidative damage and atherosclerotic lesions, have also been associated with exposure to CNTs (Li et al., 2007). *In vitro* studies on cultured human skin cells have shown that CNTs can cause oxidative stress, increased cell apoptosis and necrosis, genotoxicity, interference with mitosis, and abnormal chromosome number (Shvedova et al., 2003; Monteiro-Riviere et al., 2005; Sargent et al., 2009; Kisin et al., 2010). There are no toxicological studies on the effects of matrix-embedded CNTs: these nanocomposite particles may represent the relevant worker's exposure rather than the bulk CNTs. Further investigation of exposure during production and manipulation of CNT nanocomposites is warranted.

Current Exposure Assessment Methods

Standard methods for assessing exposure are essential to the practice of occupational health and safety to maximize protection to the worker. Exposure measurements are used to determine relationships between exposure and adverse health outcomes in epidemiological and toxicological studies and to assess exposures over time. Exposure measurements made in workplace environments are compared to occupational exposure limits for routine risk management and regulatory enforcement (Ramachandran, 2005; ACGIH, 2010). The NIOSH Manual of Analytical Methods (NMAM) describes protocols to assess personal exposure to a wide range of occupational contaminants (NIOSH, 2003).

Conventional occupational sampling methods to monitor exposure to airborne particles rely on collecting airborne particles onto filters and characterizing their mass (e.g., NMAM 0500) and bulk chemistry (e.g., NMAM 7300). Filters are mounted in generally small, lightweight samplers located in the worker's breathing zone, and a belt-mounted pump is used to pull air through the sampler. The filters are usually analyzed to determine the mass of particulate associated with its corresponding occupational standard, and the measured concentrations are compared to workplace limits. The sampler is commonly designed to match a size-selective sampling criterion based on particle aspiration into the human respiratory tract. The collection efficiency of the respiratory tract is influenced by the size of particles, and not all airborne particles will enter the respiratory system (Maynard and Jensen, 2001); therefore the dose a person may receive may differ from ambient concentrations. Dose is defined as concentration times intake rate times deposition fraction.

The inhalable sampling criterion is based on deposition of particles in the respiratory tract to reflect only those particles that may be inhaled (Vincent et al., 1990; ACGIH, 2010). The thoracic sampling criterion represents particles that can penetrate

into the tracheobronchial region as a subfraction of the inhalable aerosol (ISO, 1995). The respirable sampling criterion represents the subset of particles that when inhaled can reach the alveolar region of the lung (ACGIH, 2010). These particle-size-dependent criteria include particles that are substantially larger than 100 nm (CEN, 1993; ISO, 1995). Additionally, these criteria estimate the fraction of particles that reaches a specific area of the respiratory system and has the potential of depositing there. Although both aspiration and deposition depend on particles size, the two phenomena are not linear across the entire particle size spectrum (Koehler et al., 2009). Aspiration metrics are inadequate for estimating dose (Hodgkins et al., 1991; Esmen et al., 2002).

Respiratory Deposition of Nanoparticles

The Brownian motion of the air molecules is the primary mechanism for deposition of particles smaller than 0.3 μm. Because nanoparticles carry little mass, movement of air molecules causes them to jitter and to diffuse to surfaces (Kleinstreuer et al., 2008). This random motion is the primary mechanism that causes nanoparticles to deposit within the respiratory system (ICRP, 1994). Recent experimental work has provided insight on the deposition of nanoparticles in the respiratory tract for controlled (Heyder et al., 1986; Kim and Hu, 1998; Kim and Jaques, 2000; Jaques and Kim, 2000; Choi and Kim, 2007; Montoya et al., 2004) and uncontrolled (Daigle et al., 2003; Londahl et al., 2007, 2008 and 2009) breathing patterns. These experimental measurements demonstrated a trough-shaped total deposition curve, with minimum deposition for particles around 150 nm. Deposition of particles smaller than 150 nm increases as particle size decreases (Choi and Kim, 2007). The International Commission on Radiological Protection (ICRP) deposition model for average adult males and females under light exercise and nose-breathing conditions (ICRP, 1994) follows fairly accurately these experimental deposition patterns. Some research groups have adopted the ICRP

deposition model as a target for aerosol deposition samplers and pre-separators (Kuo et al., 2005; Koehler et al., 2009).

Samplers based on respiratory system deposition provide a suitable solution for estimation of nanoparticle dose received in the respiratory tract (Johnson and Esmen, 2004). A sampling criterion specific to nanoparticles, analogous to the respirable and inhalable criteria, and that can serve as a target curve for a deposition based sampling device is currently unavailable.

Occupational Regulation of Nanoparticles

Three major consensus groups set occupational exposure limits to protect workers' health. The American Conference of Governmental Industrial Hygienists (ACGIH) is a scientific organization with established committees that examine peer-reviewed scientific literature and publish guidelines known as Threshold Limit Values (TLVs) for safe levels of exposure to chemical and physical agents in the workplace. There is no TLV for nanoparticles, however, for biologically inert, insoluble or poorly soluble particles believed to have adverse health effects, the ACGIH has a general recommendation of a mass based TLV of 3 mg/m^3 using the respirable sampling criterion (ACGIH, 2010). The National Institute for Occupational Safety and Health (NIOSH) develops recommendations for health and safety standards called recommended exposure limits (RELs), which are not legally enforceable limits (NIOSH, 2005a), but are published and transmitted to government agencies for use in promulgating legal standards. The Occupational Safety and Health Administration (OSHA) is the U.S. government agency that sets permissible exposure limits (PELs) corresponding to the maximum legal limit for exposure to chemicals or dusts. There is no PEL specific for nanoparticles. The PEL set by OSHA for particles not otherwise regulated is 5 mg/m^3. Mass-based airborne exposure limits are typically used because mass-based concentrations have been associated with health effects of workers and have been useful

to understanding and developing dose-response relationship in animal studies (NIOSH, 2010).

Unfortunately, there is inadequate epidemiological and toxicological data to develop occupational exposure limits for nanoparticles. This lack of data is in part due to the lack of standard methods for sampling and analyzing airborne nanoparticle concentrations. Although standardization of sampling and analysis methods require overcoming several obstacles (Maynard, 2007; Papp et al., 2008), a consensus is emerging that standard methodologies are needed to measure airborne nanoparticle concentration apart from other background aerosols (Schulte et al., 2008b).

Two Proposed Sampling Strategies with Recommended Exposure Limits

Studies have suggested that ultrafine TiO_2 particles, widely used in consumer products, may be more toxic than fine TiO_2 particles at the same mass (Ferin et al., 1992; Oberdörster et al., 1992), possibly because ultrafine particles have a larger surface area than fine particles at the same mass (Oberdörster et al., 1992). Consequently, NIOSH has proposed a strategy for assessing occupational exposure to ultrafine TiO_2 (NIOSH, 2005b). NIOSH recommends a multi-tiered exposure assessment to distinguish concentrations of nano TiO_2 separately from other background aerosols. The NIOSH recommended REL for ultrafine TiO_2 is 0.1 mg/m^3 collected with filter-based respirable samplers (i.e., NMAM 0600). When respirable mass concentration measurements exceed this limit, the filters should be evaluated under transmission electron microscopy with energy dispersive X-ray spectroscopy to determine the percent TiO_2 by particle size. Then the respirable mass concentration is to be adjusted to reflect only the mass attributed to ultrafine TiO_2. This method requires the collection of two respirable samples, a costly collection of a large amount of data and a complicated process to interpret the results.

Workplace exposure to ultrafine TiO_2 is difficult to measure without a sampler specific for the collection of nanoparticles.

NIOSH has also proposed a strategy for occupational exposure to CNTs and CNFs (NIOSH, 2010). They recommend an exposure level of 7 $\mu g/m^3$ as an 8-hr time weighted average airborne respirable mass concentration for up to a 40-hr week, based on the available toxicological data from animal studies. The recommended analytical method to assess the exposure level is NIOSH method 5040, which consists of analysis for elemental carbon on respirable samples. CNTs have low density and small diameter, and this analysis method may not be sufficiently sensitive to detect low mass concentrations. The limit of detection for NIOSH method 5040 is 2 $\mu g/m^3$, with a limit of quantification of 7 $\mu g/m^3$. Furthermore, this method is not specific for differentiating elemental carbon originating from other sources such as background processes and incidental nanoparticles.

These NIOSH-proposed strategies indicate the need to measure nanoparticle airborne concentrations apart from larger particles, but also to understand the amount of exposure associated with ultrafine TiO_2 or CNTs compared to other background aerosols. Direct-reading instruments that output particle number or mass concentrations are available. However, these instruments have several limitations that make them inadequate for quantitative exposure assessment.

Direct-Read Instruments, Area Samplers and Their Limitations

Direct-read instruments have advantages associated with the ability to quickly measure particle concentrations. Some of these instruments can be used to assess the presence of nanoparticles in workplace environments (Methner et al., 2010a). There are, however, several disadvantages to their use that make them inadequate for characterization of exposure to nanoparticles.

Condensation particle counters (CPCs) grow ultrafine particles to micrometer-size droplets in a supersaturated environment so that their number concentration can be measured with a light-transmission measurement or a single-particle optical counter (Hinds, 1999). CPCs are available in portable, lightweight models; however, they have limitations in their ability to measure particle number concentrations above 100,000 particles/cm^3 due to coincidence errors. Coincidence is caused by more than one particle simultaneously in the instrument's sensitive volume, which leads to under-estimation of the particle number concentration. CPCs also respond to particles larger than 100 nm and are not adaptable to personal sampling. CPCs provide only knowledge of particle number concentrations and do not provide the ability to distinguish between incidental and engineered particles.

Scanning mobility particle sizers (SMPSs) provide number and mass concentration measurements. An SMPS consists of a differential mobility analyzer, which separates particles based on their mobility in an electrical field, paired with a CPC. SMPSs can provide the reconstruction of original ambient aerosol distributions by size with high resolution in the submicrometer size range (Liu and Deshler, 2003). These instruments have the advantage that particles do not have to be captured, they provide almost immediate particle concentration measurements, and it is not necessary to form an image of the particles in order to size or count them. They are, however, bulky (>25 kg) and expensive (~$50K), characteristics that make them not suitable as personal samplers. Additionally, their inability to distinguish between engineered and incidental nanoparticles makes them ineffective for quantitative exposure assessment. Collection of engineered nanoparticles separately from other background aerosols is necessary to properly assess the health risks associated with their inhalation.

Diffusion chargers measure the surface area of particles smaller than 1 μm. As particles come in contact with ions, an electrometer measures the amount of charge on each particle (Hinds, 1999). This charge is correlated with the particle's surface area.

Diffusion chargers are fairly portable, but they do not provide information on particle size. Electrical low-pressure impactors use a combination of diffusion charging techniques and a cascade impactor to measure the amount of charged particles corresponding to a particular aerodynamic diameter (Baron and Willeke, 2001a). However, similarly to SMPSs, electrical low-pressure impactors are large and inadequate for personal sampling.

These above samplers are useful to deploy as static area samplers, however, area samplers may not accurately reflect personal exposures because nanoparticles tend to rapidly decrease in concentration away from a source (Zhu et al., 2002). Nanoparticle concentrations near a source are generally high, and the constant bombardment of air molecules on nanoparticles makes them move and change direction rapidly, increasing their likelihood of hitting and coagulating with other particles (Hinds, 1999). Consequently, personal exposures to nanoparticles are likely to be highly heterogeneous and depend upon proximity to a source, which tends to change over an 8-hr shift because of worker's movements. Personal samplers can overcome the limitations of area samplers by collecting air samples in a worker's breathing zone and therefore better characterize an individual's exposure. A personal sampler that collects nanoparticles separately from other background particles would further support this exposure characterization effort.

Collection of Nanoparticles Separately from Larger Particles

One approach to selectively remove particles from an airstream is the combination of carefully designed inertial separators with diffusion screens. Particle behavior in a gas suspension is highly dependent upon size (Baron and Willeke, 2001b). Therefore, selective collection of nanoparticles requires the use of a combination of techniques. Particles larger than 0.5 μm carry more mass than nanoparticles and therefore are not as affected by the Brownian motion of the air molecules. Because of this greater

mass, particle inertia plays a major role in their movement and can be used to separate and collect particles of different sizes with different techniques (Marple et al., 2001).

Cyclones and impactors have been used to efficiently remove large particles from an airstream. These devices accelerate the air with the use of acceleration nozzles and cause it to flow in a spiral pattern or to abruptly change direction. Particles with sufficient inertia are unable to follow the air streamlines during these direction shifts and collect onto the walls of the device or on other internal collection substrates (Marple et al., 2001). Only those particles able to follow the air streamlines will remain airborne. The particle diameter for which 50% of the particles are collected and removed from the airstream, while all particles less than this size pass through, is called the cut-size or d_{50} (Hinds, 1999). Although impactors and cyclones have been designed to achieve nanometer cut-sizes (Hering et al., 1979; Marple et al., 1991; Chen et al., 2007), these low cut-points require extremely high pressure drops, which are not easily achievable with belt-mounted sampling pumps that are widely used for personal sampling.

Filters and screens can be used to collect nanoparticles from an airstream at relatively low pressure drops. Unlike gas molecules, when nanoparticles hit a surface, such as the fiber of a filter or a screen, they adhere and are removed from the airstream. As the air flows through a layer of fibers, the random movement of nanoparticles increases their probability of diffusing onto a fiber. Filtration theory has been thoroughly studied and developed to predict collection efficiency of fibrous filters (Fridlander, 1958; Kirsch and Fuchs, 1968). The non-uniform diameter and random fiber orientation of filters, however, makes it difficult to accurately predict particle collection efficiency (Cheng et al., 1985). Diffusion screens, which consist of woven uniform fibers, have been successfully used to collect nanoparticles (Cheng and Yeh, 1983; Cheng, 2001). Theoretical estimations of collection efficiency have been examined for diffusion screens made of stainless steel fibers (Cheng et al., 1985). Their uniform fiber size and

arrangement make diffusion screens a desirable collection substrate; metal fibers, however, pose several analytical limitations.

Analysis of particles collected on a filtration media often requires the particles to be separated from the fibers through digestion or ashing of the fibers (Grohse, 1999). Stainless steel fibers are difficult to digest without also permanently damaging the particles collected. Nylon mesh screens present an advantageous alternative to metal screens because of the ease of dissolving nylon fibers compared to metal fibers.

Diffusion screens, however, are not size selective sampling devices as both nanoparticles and larger particles collect onto their fibers. Gorbunov et al. (2009) developed a size-selective sampler that uses an impactor to remove large particles and nylon mesh screens to collect nanoparticles. They analyzed the nanoparticles apart from larger particles by treating the nylon mesh screens in *aqua regia* and subjecting them to microwave digestion. The large size of this sampler, however, limits its use to area sampling.

Shortcomings of the Literature

Understanding and mitigating health risks posed by nanoparticles in the workplace require knowledge of relevant workers' exposures. As nanoparticles are incorporated in matrix structures to form nanocomposite materials, workers of production facilities may be exposed to both bulk engineered nanoparticles and to matrix-embedded nanoparticles. The toxicity of these matrix-embedded particles may be very different from that of the bulk material. It is necessary to characterize exposure to airborne particles emitted during manufacturing of nanocomposite materials. Furthermore, local exhaust ventilation conditions need to be assessed to determine their effectiveness to control exposure during manipulation and mechanical processing of nanocomposite materials. Characterization of exposure to nanocomposite materials containing CNTs is particularly important because of their widespread use in manufacturing facilities and the

currently ongoing effort to set exposure standards for CNTs (NIOSH, 2010). Research is needed to estimate and determine risks of exposure to CNT nanocomposite materials.

There is a need for personal samplers capable of capturing airborne nanoparticles apart from other aerosols present in workplace atmospheres. Currently available 8-hr filter-based samplers (e.g., respirable samplers) cannot separate the mass of nanoparticles from that of larger particles. Selective collection of nanoparticles is necessary to properly assess the health risks associated with their inhalation. Additionally, accurate estimation of nanoparticle exposures via inhalation would be enhanced by collection of nanoparticles with a sampler that matches nanoparticle deposition in the respiratory system. Understanding personal exposures to nanoparticles will assist in the development of future toxicological and epidemiological studies.

Characterization of nanoparticle exposure requires particle collection on substrates suitable for analytical techniques. Nylon mesh screens provide an inexpensive, disposable collection substrate that can be ashed or digested for multielemental analysis of particulate matter collected leaving minimal interfering residuals. These screens appear to be a suitable diffusion media for incorporation into a personal sampler for nanoparticles. The collection efficiency of nylon mesh screens for nanoparticles, and the ability of theoretical models to estimate their collection efficiency, however, have not been investigated. Furthermore, as engineered nanoparticles are present in workplace environments in various morphologies, the extent of the effect of particle morphology on the collection efficiency of nylon mesh screens needs to be investigated.

Specific Aims

The work presented in this doctoral dissertation attempts to fill the aforementioned shortcomings of the literature. The overall goals of this dissertation are to provide knowledge of worker's exposure to nanoparticles and to assist in the development of standard methods to measure personal exposure to nanoparticles in

workplace environments. To achieve the first goal, a field study was conducted in Aim 1. The second goal was achieved in two laboratory studies described in Aims 2 and 3.

Aim 1. Characterize airborne particles during handling of bulk CNTs and the mechanical processing of CNT composites, and evaluate the effectiveness of local exhaust ventilation systems to capture airborne particles generated by sanding CNT nanocomposites. A manuscript resulting from this work was published in the February 2011 issue of the *Journal of Occupational and Environmental Hygiene*, volume 8, pages 86-92.

Aim2. Experimentally measure pressure drop and single-fiber efficiency by size of submicrometer particles for nylon mesh screens, determine how particle morphology affects collection efficiency of nylon mesh screens and evaluate filtration theory to estimate their collection efficiency for submicrometer particles. The target journal for this work is the *Journal of Aerosol Science*.

Aim 3. Develop a sampling criterion for nano-particulate matter (NPM) based on nanoparticle deposition in the respiratory system. Develop and test the performance of a personal nanoparticle respiratory deposition sampler that selectively collects nanoparticles apart from larger airborne particles and samples according to the NPM criterion. The target journal for this work is *Environmental Science and Technology*.

CHAPTER II
CHARACTERIZATION AND CONTROL OF AIRBORNE PARTICLES EMITTED DURING PRODUCTION OF EPOXY / CARBON NANOTUBE NANOCOMPOSITES[1]

Abstract

This work characterized airborne particles that were generated from the weighing of bulk, multi-wall carbon nanotubes (CNTs) and the manual sanding of epoxy test samples reinforced with CNTs. It also evaluated the effectiveness of three local exhaust ventilation (LEV) conditions (no LEV, custom fume hood and biosafety cabinet) for control of particles generated during sanding of CNT-epoxy nanocomposites. Particle number and respirable mass concentrations were measured using an optical particle counter (OPC) and a condensation particle counter (CPC), and particle morphology was assessed by transmission electron microscopy. The ratios of the geometric mean (GM) concentrations measured during the process to that measured in the background (P/B ratios) were used as indices of the impact of the process and the LEVs on observed concentrations. Processing CNT-epoxy nanocomposites materials released respirable size airborne particles (P/B ratio: weighing = 1.79; sanding = 5.90) but generally no nanoparticles (P/B ratio ~1). The particles generated during sanding were predominately micrometer-sized with protruding CNTs and very different from bulk CNTs that tended to remain in large (>1 μm), tangled clusters. Respirable mass concentrations in the operator's breathing zone were lower when sanding was performed in the biological safety cabinet (GM = 0.20 $\mu g/m^3$) compared to those with no LEV (GM = 2.68 $\mu g/m^3$) or those when sanding was performed inside the fume hood (GM = 21.4 $\mu g/m^3$; p-value <

[1]Manuscript published in the February 2011 issue of the *Journal of Occupational and Environmental Hygiene*, volume 8, pages 86–92.

0.0001). The poor performance of the custom fume hood used in this study may have been exacerbated by its lack of a front sash and rear baffles and its low face velocity (0.39 m/sec).

Introduction

Carbon nanotubes (CNTs) can be incorporated into polymeric materials to form nanocomposite materials (Lau and Hui, 2002). Compared to the polymeric material alone, these nanocomposites have increased resistance to strain and tensile strength, improved electrical and thermal properties, and enhanced ability to bridge cracks (Lau and Hui, 2002). Products that incorporate CNT nanocomposites include sporting goods, automotive parts and electronics (Hansen et al., 2008), and the number of industrial and commercial applications of these nanocomposites are projected to increase as their production cost decreases (Lam et al., 2006; Hansen et al., 2008).

Workplace exposure to airborne CNTs may represent an occupational hazard (Tejral et al., 2009). Toxicological studies have associated exposure to CNTs with adverse pulmonary (granulomas, fibrosis, diminished resistance to pathogenic attacks) (Lam et al., 2004; Warheit et al., 2003; Muller et al., 2005; Shvedova et al., 2003), cardiac (oxidative damage, atherosclerotic lesions) (Li et al., 2007) and dermal health effects (oxidative stress, increased cell apoptosis and necrosis) (Shvedova et al., 2003; Monteiro-Riviere et al., 2005).

The production of CNT nanocomposites involves the processing of bulk CNTs, which are CNTs not incorporated in a matrix and CNTs embedded in a polymer matrix such as epoxy resin (Lam et al., 2006). Weighing or pouring bulk CNTs has been observed to release only small quantities ($<53 \mu g/m^3$) of airborne particles in laboratory (Baron et al., 2003; Maynard et al., 2004) and field conditions (Maynard et al., 2004). Appreciable respirable concentrations have been observed only after vigorous agitation (Maynard et al., 2004). In contrast, the mechanical processing of CNT nanocomposites

may impart greater energy to produce appreciable quantities of airborne particles during typical workplace operations. Köhler et al. (2008) suggest that the way CNTs are incorporated in the matrix and the mechanism by which a nanocomposite degrades determine the likelihood and form of their release. Mechanical processing of nanocomposites may release micrometer-sized aggregate polymer-CNT particles or CNTs in a dispersive nanoparticulate state (Lam et al., 2006; Köhler et al., 2008).

Laboratory enclosures have been designed to protect workers from exposure during handling and processing of hazardous substances. The effectiveness of fume hoods as a control measure during *nanoparticle* manipulation has been investigated by Tsai et al. (2009b). They measured airborne concentration while dry nanopowders were handled under three fume hoods and a range of operating conditions (variable sash height and face velocity). Their results showed that the release of airborne nanoparticles from within a fume hood into the laboratory environment is highly dependent upon hood design and hood conditions (sash height, face velocity). Further, they suggested that more sophisticated hood designs, such as air-curtain biosafety cabinets, may be more effective in containing nanoparticles (Tsai et al., 2009b). The effectiveness of enclosures to contain particulate release, however, has not been investigated during the manipulation of *nanocomposite* materials containing CNTs.

The goals of this study were 1) to characterize airborne particles during handling of bulk CNTs and the mechanical processing of CNT nanocomposites and 2) to evaluate the effectiveness of local exhaust ventilation (LEV) hoods to capture airborne particles generated by sanding CNT nanocomposites.

Methods

Manufacturing Process

This study was conducted in a facility that produces test samples composed of epoxy reinforced with CNTs. The test samples are rectangular sticks of CNT-epoxy with dimensions of 12.5 x 1.3 x 0.5 cm that are used to evaluate the effect of formulation variables on the properties of the nanocomposites. Specific details of this process are not reported at the request of the manufacturer; only the details required to interpret results from an occupational health and safety perspective are presented.

To produce the test samples, bulk multi-wall CNTs with 10-50 nm outer diameter and 1-20 μm length (Baytubes, Bayer Material Science LLC, Pittsburg, PA) are weighed and mixed with epoxy. This mixture is poured into a mold designed to produce four test samples at a time and baked in an oven for several hours. Then the hardened nanocomposite test samples are broken apart manually, and each one is manually sanded to remove excess material until final dimensions are achieved.

Airborne Particle Measurement and Characterization

Airborne particle number and respirable mass concentrations were measured with two direct-read instruments: a condensation particle counter (CPC), and an optical particle counter (OPC). The CPC (model 3007, TSI Inc., St. Paul, MN) was used to provide total particle number concentration for particles that ranged in diameter from 0.01 to 1 μm. The OPC (Portable Dust Monitor series 1.108, GRIMM Technologies, Douglasville, GA) was used to provide particle number concentration in 15 size channels from 0.3 to 20 μm.

Respirable mass concentrations were estimated from the OPC data using the respirable particulate matter (RPM) fraction defined by ACGIH (2010). This fraction

consists of those particles that were captured as specified by the following collection efficiency:

$$\mathrm{RPM}(d_{OPC,i})=0.5[1+\exp(-0.06d_{OPC,i})]\cdot[1-\mathrm{F}(x)], \quad (2\text{-}1)$$

where $d_{OPC,i}$ is the midpoint diameter of the OPC ith channel in μm, and F(x) is the cumulative probability function of the standardized normal variable x,

$$x = \frac{\ln\left(\frac{d_{OPC,i}}{4.25}\right)}{\ln(1.5)}.$$

For each OPC measurement, respirable mass concentration, M_R, was calculated as:

$$M_R = \sum_{1}^{15} \frac{\pi}{6} d_{OPC,i}^3 \rho N_{OPC,i} RPM\left(d_{opc,i}\right), \quad (2\text{-}2)$$

where $N_{OPC,i}$ is the number concentration indicated by the OPC for a given size channel i, and ρ is the particle density (2.25 g/cm^3 for epoxy resin).

The morphology of representative airborne particles was observed by transmission electron microscopy (TEM). Samples for microscopy were collected with a sampler similar to that described by Tsai et al. (2009b). It consisted of a copper TEM grid (300 mesh with carbon type-b film, 01813-F, Ted Pella, Inc., Redding, CA) affixed with carbon tape onto the center of the face of a polycarbonate membrane filter (E0055-MB, SPI Supplies, West Chester, PA). This filter was then mounted in an open-face conductive filter cassette (25 mm, 225-3-23, SKC Inc., Eighty Four, PA). Airflow was pulled through the sampler with a personal sampling pump (Buck Basic-5, A.P. Buck Inc., Orlando, FL) at 1 L/min. The copper grids were analyzed under TEM (JEM-1230; JEOL USA Inc., Peabody, MA) to characterize the size and morphology of a representative subset of the collected airborne particles.

Process Measurements

Airborne concentrations were measured during two processes: weighing bulk CNTs and sanding epoxy nanocomposite test sticks. To simulate weighing, 600 mg of the bulk CNTs was transferred by scooping material between two 50 mL beakers for three five-minute intervals at a rate of ~ 1 scoop/sec. Each scoop contained approximately 50 mg of CNT material. These tests were conducted in a filtered glove box with the CPC and OPC located inside the glove box with their inlets positioned 7.5 cm away from and oriented towards the weighing process. Background concentrations were measured for 15 min inside the glove box before the process began. One TEM sample was collected inside the glove box during the entire weighing process. Additional TEM samples were prepared by artificially depositing CNTs on TEM grids by dropping them from a laboratory spatula on to the TEM grids.

To study the sanding process, an operator manually sanded epoxy test sticks that contained 2% by weight CNTs with sandpaper (220 grit, model 20240, 3M, St Paul, MN). The operator wore a full-face respirator with particulate filters (Full Facepiece 6700, 3M, St Paul, MN). Aerosol concentrations were measured for 15-30 min in two locations: adjacent to the sanding process and in the operator's breathing zone. For process measurements (termed 'inside enclosure' measurements), the inlets of the CPC and OPC were positioned 7.5 cm away from and oriented towards the sanding process. For breathing zone measurements, two electrically conductive, flexible tubes (1.4 m long with an inner diameter of 0.48 cm) were used to transport the aerosol from just outside of the respirator to a second CPC and OPC. TEM samples were collected at 7.5 cm from the sanding surfaces. Diffusion losses introduced by the presence of the sampling tube on CPC measurements were estimated from theory to be 23% for 10 nm particles and less than 5% for particles larger than 40 nm (Brockmann, 2001). The bias introduced by the

sampling tube on respirable mass concentration was estimated to be less than -5% (Peters and Volkwein, 2003).

For sanding, source and breathing zone measurements were taken under three LEV conditions (no LEV, a custom fume hood, and a biological safety cabinet). With no LEV, the sanding process was conducted on a 1.2 m by 2.2 m work table. The custom fume hood consisted of a simple vented enclosure that allowed airflow along all sides of the back panel. The custom fume hood had no front sash or rear baffles, and its dimensions were 0.57 m (height) by 1.33 m (width) by 0.76 m (depth). The face velocity of the hood was measured at the center of 21 equally spaced positions according to the procedures outlined by ANSI/ASHRAE 110-1995 (ANSI/ASHRAE, 1995). The biological safety cabinet was class II type A2 (Sterilgard III 303, Baker Co., Sanford, ME) with dimensions of 0.53 m (height) by 0.7 m (width) by 0.45 m (depth). The cabinet was tested for performance evaluation and operated with a 20 cm (8 inch) sash height. During all tests, the LEV contained no additional equipment that may have blocked airflow, and no other equipment external to the LEV was operated in the room that may have generated airborne particles. Background measurements were taken for 30 min prior to each test in the rooms as well as inside the LEV enclosures in the same location as the process measurements.

Data Analysis

All particle number and respirable mass concentrations were tested for normality using Shapiro-Wilk test before and after performing a log transformation. The geometric mean (GM) and geometric standard deviation (GSD) were obtained for all number and respirable mass concentrations at each condition tested. Process-to-background ratios (P/B ratios) were calculated for all measurements with the formula

$$P/B\ Ratio = \frac{Process\ GM\ Concentration}{Background\ GM\ Concentration}. \quad (2\text{-}3)$$

Breathing zone and process GM concentrations were matched with their respective background measurements.

Analysis of variance (ANOVA) was used to compare respirable mass concentrations measured in the operator's breathing zone during the sanding process with and without control measures. Not all data passed the Shapiro-Wilk test for normality; therefore the concentrations were further compared by Kruskal-Wallis nonparametric test. The Tukey-Kramer Honestly Significant Difference (HSD) test was used to compare GM concentrations observed for different LEV conditions.

Results

The GM and GSD of the observed particle number and respirable mass concentrations are summarized by process in Table 2-1. Table 2-2 presents GM and GSD of the particle number and respirable mass concentrations obtained under various LEV conditions during the sanding process. The P/B ratios indicate the relative impact of the process (weighing or sanding) or of the LEV on observed concentrations. Values near unity indicate that the process generated little aerosol, whereas values progressively greater than unity indicate that the process increased aerosol concentrations.

Influence of Process on Airborne Concentrations

The weighing process contributed little to observed particle number concentrations (Table 2-1; P/B ratio = 1.06). It did influence mass concentration (Table 2-1; P/B ratio = 1.79), although very low computed respirable mass concentrations were observed inside the glove box during weighing (GM = 0.03 $\mu g/m^3$) and in background measurements (GM = 0.02 $\mu g/m^3$). Electron microscope analysis revealed no CNT particles deposited on the TEM grids during the weighing process. The CNTs artificially deposited onto TEM grids appeared as large bundles (>1 μm) containing many tangled nanotubes (Figure 2-1).

During the sanding process, nanoparticle number concentrations were negligible compared to background concentrations (Table 2-1; P/B ratio = 1.04), indicating that nanoparticles did not disperse to any great extent. Respirable mass concentrations, however, were elevated in the breathing zone (Table 2-1; P/B ratio = 5.90).

The particles collected during sanding were predominantly large (>300 nm) and irregular in shape (a representative particle is shown in Figure 2-2). These particles commonly had protuberances that emerged from the perimeter of the particles. These protuberances had an outer diameter between 10 and 50 nm, which is consistent with that of the CNTs.

Influence of Local Exhaust Ventilation During Sanding

Particle number concentrations measured in the breathing zone during sanding were negligible compared to background for all three LEV conditions (Table 2-2; breathing zone P/B ratios: custom fume hood = 1.03, no LEV = 1.04, biosafety cabinet = 1.05). The P/B ratios were dissimilar for process measurements made inside enclosures (Table 2-2; inside enclosure). Inside the fume hood the P/B ratio was 1.01, very close to unity. Inside the biosafety cabinet, the P/B ratio was 2.35, indicating a 135% increase in number concentrations; however, the actual concentrations in this condition were very close to zero (GM = 0.06 particles/cm^3), with a maximum of 8 particles/cm^3.

Respirable mass concentrations in the worker's breathing zone varied substantially by LEV (Table 2-2; breathing zone). Figure 2-3 presents box-and-whisker plots of these breathing zone measurements. The ANOVA test reported significant differences between the three LEV conditions (p-value <0.0001 confirmed by Kruskal-Wallis nonparametric test), and the Tukey-Kramer HSD test confirmed that all pair-wise comparisons were significantly different (p-values <0.00001). Inside the LEV enclosures, respirable mass concentrations were considerably higher than background levels. The P/B

ratio was 28.6 for the fume hood LEV and 3.47 for the biosafety cabinet LEV (Table 2-2; inside enclosure).

The average face velocity of the fume hood, measured with a thermal anemometer (VelociCalc 8360, TSI, Inc. St. Paul, MN), was 0.39 m/sec (76 ft/min). As shown in Figure 2-4, the air velocity near the lower part of the hood's face, closer to the sanding surface, was on average 0.23 m/sec (45 ft/min) while in the upper area it averaged 0.45 m/sec (88 ft/min), with maximum flow at 0.60 m/sec (118 ft/min) in the upper central area of the hood's face.

Discussion

Processing CNT-nanocomposite materials releases respirable size airborne particles but generally no nanoparticles. The finding that P/B ratios for number concentration were near unity (Table 2-1) indicates that nanoparticles did not disperse to any great extent either when weighing bulk CNTs or during the sanding process. This result is consistent with the work of Baron et al. (2003) and Maynard et al. (2004) who found that CNTs are difficult to separate into isolated particles and that the particles released during handling of bulk CNTs tend to be larger than 1 μm. Baron et al. also found that aerosol generation rates were typically two orders of magnitude lower when comparing CNTs to fume alumina bulk materials (a material formed from nanometer-sized primary particles with similar low bulk density to CNTs).

Respirable mass concentrations in the breathing zone of the operator were elevated compared to background during sanding without LEV (P/B ratio = 5.90). However, the geometric mean (GM = 2.68 $\mu g/m^3$) was considerably lower than the only applicable occupational standard, the recommended American Conference of Governmental Industrial Hygienists (ACGIH, 2010) respirable particles threshold limit value for particles not otherwise specified (PNOS TLV – 3000 $\mu g/m^3$).

The P/B ratio for respirable mass concentration of 1.79 measured during the weighing process (Table 2-1) appears to indicate that the process did influence mass concentrations. However, very low respirable mass concentrations were observed during weighing (0.03 $\mu g/m^3$), and when concentrations are extremely low, even small fluctuations will be reflected as a substantial increase in the P/B ratios. Such small fluctuations may be related to normal background variability (Background GM 0.02 $\mu g/m^3$, GSD 2.06) rather than actual increases in respirable mass concentrations while weighing CNTs.

The morphology of particles generated during sanding CNT-epoxy nanocomposites was very different from the bulk CNTs (Figures 2-1 and 2-2). The particles collected in the operator's breathing zone during sanding were micrometer-sized with protruding features (Figure 2-2). Their morphology suggests that they are epoxy particles and that the protrusions are embedded CNTs which extend outward beyond the perimeter of the particle. No CNTs were observed free from composite material for the manual sanding studied in this work. It is, however, possible that free CNTs are generated and would be observed at higher concentrations or when mechanical sanding is performed.

The fact that free CNTs were not liberated from the epoxy is consistent with research on asbestos-containing materials. Asbestos fibers that are encapsulated or bonded with other materials, such as resins, have been found to have a limited potential for airborne release (Mowat et al., 2000). Aggressive manipulation, such as sanding, sawing or drilling of polymer matrices containing asbestos fibers has been found to produce airborne concentrations of asbestos that are less than 1-2% lower than the historical standards set by OSHA and ACGIH for worker protection, and at least three-fold less than the current 8-hour TWA occupational exposure limits (0.1 fiber/cm^3) (Mowat et al., 2000).

No particles were found on the TEM samples collected during the raw CNT weighing simulation of this study. The CNTs that were artificially deposited onto TEM grids appeared mainly as large (>1 μm), tangled clusters. Similar large clusters were observed to deposit on the inner surface of the glove box during the process simulation. In contrast, exposure to asbestos fibers has been found to occur when workers handle and process raw asbestos fibers or friable products such as insulation (Mowat et al., 2000).

Toxicological studies have focused to date on the adverse health effects associated with exposure to bulk CNTs. Our findings suggest that inhalation exposure to bulk CNTs is likely to be low in activities such as weighing. In contrast, sanding does generate respirable particles that can enter a worker's breathing zone, and these particles were very different morphologically than bulk CNTs. Given the lack of toxicity data for this type of particles, it cannot be determined whether exposure to the sanding particles generated at the concentrations measured in this study presents a risk to workers' health. Precautions such as the use of personal protective equipment or working within a hood that meets design specifications and standards or a biological safety cabinet should be taken until health effects are better understood.

LEV conditions had a substantial influence on respirable mass concentrations in the operator's breathing zone. Breathing zone concentrations were elevated when sanding took place inside the custom fume hood (Table 2-2 and Figure 2-3). The facemask of the operator performing the sanding task in the custom hood was consistently covered with particles that had to be removed with the use of dry wipes in order to improve visibility.

The poor performance of the custom hood used in the current study may have been exacerbated by its lack of a front sash, its lack of rear baffles to distribute the airflow (Wunder, 2000) and its low face velocity. The ACGIH recommends an inward face velocity for a fume hood of 0.4-0.5 m/sec (80-100 ft/min) with a velocity difference at any point in the face opening no greater than 10% of the average velocity (ACGIH, 2007). The maximum air velocity of the custom fume hood used in this study (0.60

m/sec; 118 ft/min) was 200% greater than its average velocity of 0.23 m/sec (45 ft/min). The uneven velocity distribution may have affected airflow patterns around the worker and the ability of the custom fume hood to remove particles from the operator's breathing zone. Operator movements may increase air turbulence inside a hood, compromising its effectiveness to remove contaminants and pulling dust particles towards the operator (Wunder, 2000). Similar results were found by Tsai et al. (2009b), who observed the transport of alumina nanoparticles from within a fume hood that met ACGIH criteria for face velocity into the breathing zone of the operator. However, Tsai et al. (2009b) also found that containment in a conventional fume hood is highly dependent upon its design and operating conditions. These findings corroborate the importance of effective hood design details such as the use of air currents and how eddy currents may influence hood containment efficiency.

In contrast, the breathing zone respirable mass concentrations (Table 2-2 and Figure 2-3) were significantly lower when sanding was conducted in the biosafety cabinet compared to the other LEV conditions. Airflows are substantially different in biosafety cabinets, mainly because of the presence of a front suction slot, which creates an air curtain across the front aperture (Kruse et al., 1991; Huang and Chou, 2009). This air curtain separates the outside atmosphere and the inside space of the cabinet, preventing escape of contaminants from containment. These observations suggest that biosafety cabinets may be an appropriate control measure to contain exposure during sanding of CNT-reinforced epoxy.

The P/B ratio less than unity observed during sanding with the biosafety cabinet LEV (Table 2-2; 0.66) suggests that the mass concentration was greater in the background than that during sanding. This observation was likely due to fluctuations in background concentrations and to the extremely low mass concentrations (GM = 0.20 $\mu g/m^3$). Small fluctuations in background concentrations inside the biosafety cabinet could have substantially affected the P/B ratio, but do not appear to be related to the

sanding task. An analogous situation applies to the near zero particle number concentrations inside the biosafety cabinet (Table 2-2; GM = 0.06 particles/cm^3) and its associated high P/B ratio (2.35).

There are several limitations of this work. The fact that this work was conducted in an industrial facility under 'as is' conditions limited our ability to control experimental variables and perform extensive repeated measurements. Exposures during sanding may be highly variable depending on how forcefully the sanding is performed and whether it is done continuously over a 30-minute period. Future studies should investigate how process details affect particulate generation and establish how the amount of material dispersed from the sandpaper contributes to aerosol measurements. Although aerosol concentrations for all three LEV conditions were continuously logged over a 15-30 minute period, the statistical parameters may not be representative of what is expected when a task is repeated several times. Lastly, it may be difficult to generalize the findings of this work to nanocomposite materials containing non-fibrous nanoparticles since non-fibrous particles may be more easily aerosolized than fibrous particles.

Conclusions

This study demonstrated that weighing bulk CNTs and sanding epoxy containing CNTs generates few airborne particles that are nano-sized. Furthermore it was demonstrated that sanding epoxy containing CNTs may generate micrometer-sized particles with CNTs protruding from the main particle core. These epoxy particles with embedded CNTs, and not the bulk CNTs, appear to represent the relevant worker's exposure during the production process examined in this study. The toxicity of epoxy particles containing CNTs is unknown and should be the topic of future studies. Without such knowledge, precautions, such as the use of LEV, should be applied to avoid exposures resulting from manipulating epoxy that contains CNTs. This study also found that a biological safety cabinet was more effective than a custom fume hood to control

airborne exposures resulting from sanding epoxy containing CNTs. Future studies should characterize exposures that occur throughout the various steps involved in the manufacturing of products that contain nanomaterials.

Table 2-1: Particle number and respirable mass concentrations observed during the weighing and sanding processes.

Number Concentration				
Process	**N**	**GM (particles/cc)**	**GSD**	**P/B Ratio**
Weighing	300	166	1.08	1.06
Sanding	100	3889	1.48	1.04
Respirable Mass Concentration				
Process	**N**	**GM ($\mu g/m^3$)**	**GSD**	**P/B Ratio**
Weighing	51	0.03	3.50	1.79
Sanding	130	2.68	6.57	5.90

Note: N represents the number of points logged by the instruments during one run.

Table 2-2: Particle number and respirable mass concentrations during sanding with and without local exhaust ventilation (LEV).

Number Concentration								
	Breathing Zone				Inside Enclosure			
LEV	**N**	**GM #/cc**	**GSD**	**P/B Ratio**	**N**	**GM #/cc**	**GSD**	**P/B Ratio**
Custom Hood	210	1989	1.07	1.03	211	1742	1.05	1.01
None	100	3889	1.48	1.04	119*	3765*	1.07*	1.01*
Biosafety Cabinet	101	1350	1.07	1.05	108	0.06	2.41	2.35
Respirable Mass Concentration								
	Breathing Zone				Inside Enclosure			
LEV	**N**	**GM µg/m³**	**GSD**	**P/B Ratio**	**N**	**GM µg/m³**	**GSD**	**P/B Ratio**
Custom Hood	190	21.4	5.85	24.4	93	31.5	12.1	28.6
None	130	2.68	6.57	5.90	80*	10.6*	7.02*	23.2*
Biosafety Cabinet	101	0.20	2.12	0.66	108	0.03	39.7	3.47

Note: N represents the number of data points logged by the instruments during one run.
*For LEV=none (work table), inside enclosure measurements were taken adjacent to the source in the same relative location as those taken inside the custom fume hood and the biosafety cabinet.

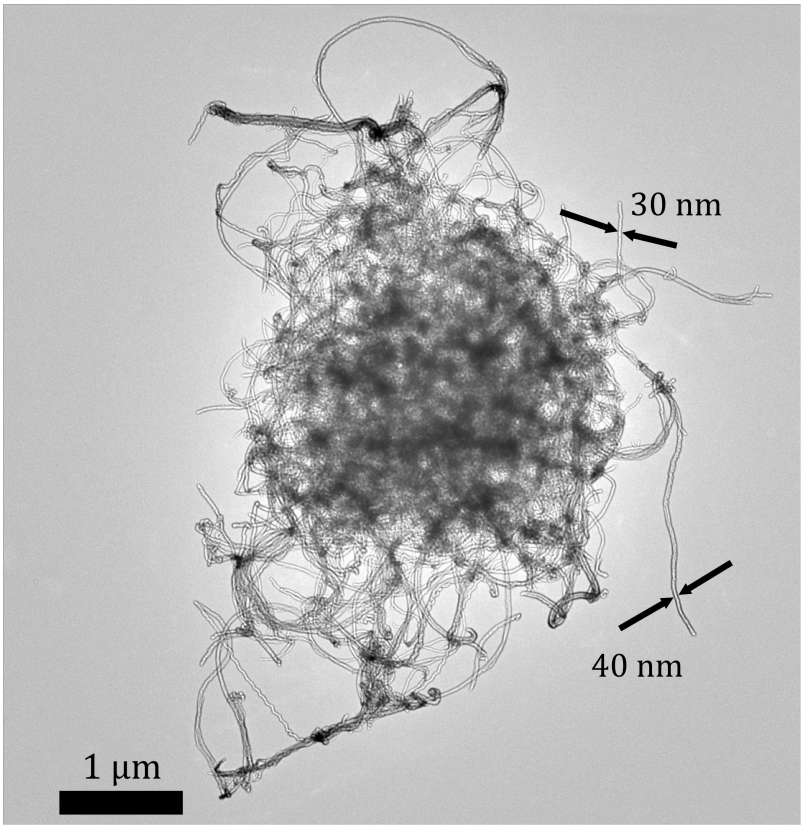

Figure 2-1: Bulk 10-50 nm outer diameter multi-wall CNTs with many tangled nanotubes.

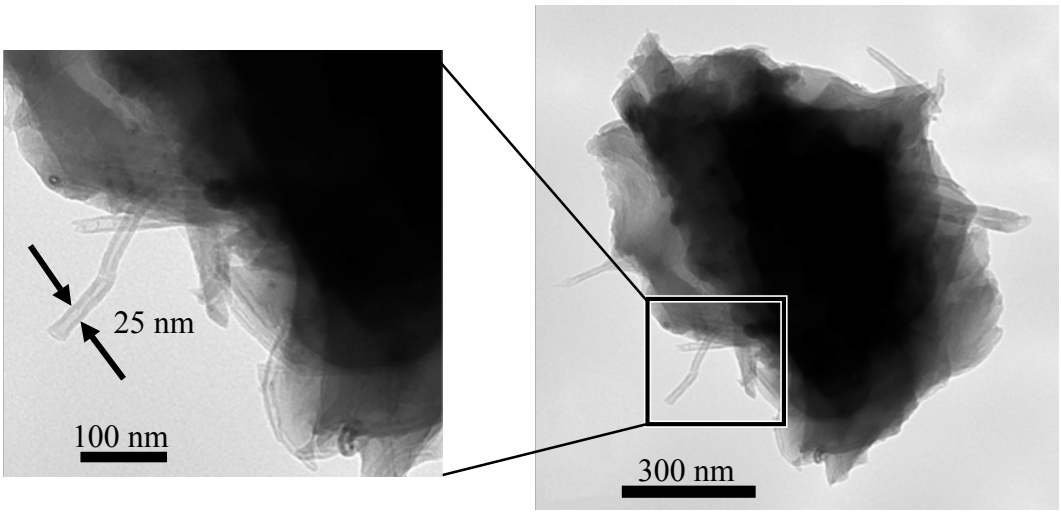

Figure 2-2: Sanding particle with detail of protruding fibers (TEM image).

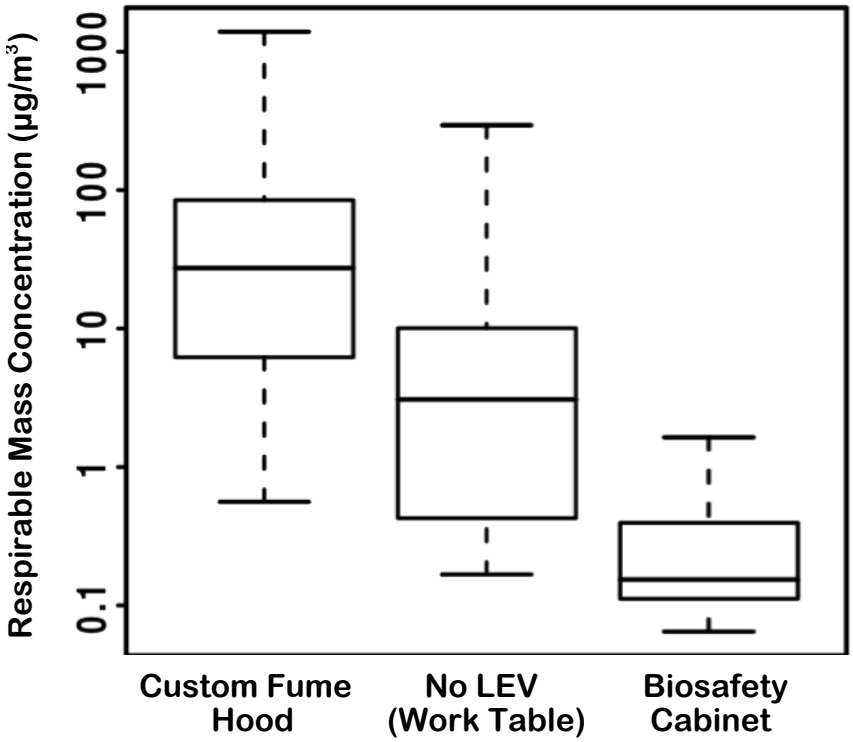

Figure 2-3: Box-and-whisker plot of log-transformed respirable mass concentrations.

Note: Box parameters represent median, lower and upper quartiles; whiskers represent sample minimum and maximum.

0.14 (28)	0.48 (95)	0.59 (116)	0.54 (107)	0.60 (118)	0.55 (109)	0.22 (43)
0.30 (59)	0.35 (68)	0.37 (72)	0.44 (86)	0.40 (78)	0.39 (77)	0.24 (48)
0.31 (60)	0.24 (47)	0.20 (40)	0.27 (53)	0.23 (45)	0.19 (39)	0.14 (28)

19 cm

19 cm

Figure 2-4: Air velocities in m/sec (ft/min) measured at the face of the custom fume hood.

CHAPTER III

SUBMICROMETER PARTICLE COLLECTION EFFICIENCY FOR NYLON MESH SCREENS

Abstract

Mesh screens composed of nylon fibers leave minimal residual ash and produce no significant spectral interference when ashed for spectrometric examination. These characteristics make nylon mesh screens attractive as a collection substrate for nanoparticles. A theoretical single-fiber efficiency expression developed for wire-mesh screens was evaluated for estimating the collection efficiency of submicrometer particles for nylon mesh screens. Pressure drop across the screens, the effect of particle morphology (spherical and highly fractal) on collection efficiency and single-fiber efficiency were evaluated experimentally for three pore sizes (60, 100 and 180 μm) at three flow rates (2.5, 4 and 6 Lpm). The pressure drop across the screens was found to increase linearly with superficial velocity. The collection efficiency of the screens was found to vary by less than 4% regardless of particle morphology. Single-fiber efficiency calculated from experimental data was in good agreement with that estimated from theory for particles between 40 and 150 nm but deviated from theory for particles outside this size range. New coefficients for the single-fiber efficiency model were identified that minimized the sum of square error (SSE) between the values estimated with the model and those determined experimentally. Compared to the original theory, the SSE calculated using the modified theory was at least one order of magnitude lower for all screens and flow rates with the exception of the 60-μm pore screens at 2.5 Lpm, where the decrease was threefold.

Introduction

Wire-mesh screens have been widely used to sample submicrometer particles from aerosol streams and for determination of particle size distributions (Gentry and Choudhary, 1975; Emi et al., 1982; Fu et al., 1990). The compact surface with uniform thickness, fiber diameter, pore size and packing density of wire screens provides a consistent airflow and uniform particle collection. Stainless steel wire screens are useful as diffusion cell material in screen-type diffusion batteries for measuring number, mass or radioactivity concentrations at the inlet and outlet of each cell (Sinclair and Hoopes, 1975; Yeh et al., 1982; Cheng, 2001).

Cheng et al. (1985) investigated collection efficiency for mesh screens consisting in a single layer of woven from stainless steel wire. They found that particle collection efficiency measured experimentally was in good agreement with filtration theory expressions by Kirsch and Fuchs (1967 and 1968) and Kirsch and Stechkina (1978) adapted for wire screens (Cheng et al., 1980; Cheng and Yeh, 1980). The efficiency of a screen of a given thickness is obtained from the calculation of the number of particles of a given dimension deposited on a unit length of fiber (Kirsch and Stechkina, 1978). The dimensionless particle deposition rate per unit length of fiber is defined as single-fiber efficiency, and the overall efficiency of a screen is a function of the single-fiber efficiency (Hinds, 1999). Compared to regular filter media, stainless steel mesh screens can be cleaned and reused multiple times. However, they are not well suited for chemical analysis because the metal wires are difficult to digest and analyze separately from the particles that are collected on their surface (Solomon et al., 2001).

Nylon mesh screens offer distinct advantages over stainless steel wire screens. Nylon mesh screens consist of rows of a single layer of parallel equidistant nylon fibers with uniform diameter interwoven at 90˚ angles with pore openings ranging between 10 and 180 μm. Nylon mesh screens provide an inexpensive disposable collection substrate

that can be ashed or digested for multielemental analysis of the particulate matter collected on the screens, such as atomic absorption spectroscopy and inductively coupled plasma-mass spectrometry (Northington, 1987; Grohse, 1999). Nylon fibers have been found to leave minimal residual ash and produce no significant spectral interference when ashed for spectrometric examination (Tuchman et al., 2008). Gorbunov et al. (2009) employed nylon screens in a size-selective particle collector. They analyzed the particles collected by the instrument by treating the nylon mesh screens in *aqua regia* and subjecting them to microwave digestion.

The collection efficiency of nylon mesh screens, however, has only been tested for micrometer-sized particles (Yamamoto et al., 2005). The efficiency of nylon mesh screens to collect submicrometer particles has not been investigated. Furthermore, the ability of theoretical models to estimate collection efficiency of nylon screens for submicrometer particles has not been investigated. Particle size, particle morphology and several other fluid (flow rate, temperature, pressure) and screen (thickness, packing density, fiber diameter) characteristics play an important role and should be factored in the estimation of a screen's collection efficiency when using filtration theory (Friedlander, 1958). The effect of morphology on collection efficiency for nylon mesh screens is not known; however, evidence for filters suggests that morphology may have an important effect. Kim et al. (2009) investigated the effects of particle morphology on particle deposition in fibrous filter media and found that agglomerates with mobility diameters larger than 100 nm experience greater collection than spherical particles with the same mobility diameters. For particles smaller than 100 nm, where diffusion is the predominant collection mechanism, collection efficiency was similar regardless of particle morphology (Kim et al., 2009).

The goal of this study was to evaluate filtration theory applied to nylon mesh screens for estimating collection efficiency of submicrometer particles. A laboratory study was conducted to experimentally measure pressure drop and single-fiber efficiency

by particle size. These data were used to modify filtration theory to improve collection efficiency estimates of nylon mesh screens for submicrometer particles. A separate laboratory experiment was conducted to determine whether submicrometer particle morphology affects the collection efficiency of nylon mesh screens and should be included in the filtration theory model.

Methods

Screens

Mesh screens composed of woven nylon 6-6 fibers with pore sizes 60, 100, and 180 μm (models NY60, NY1H, NY8H; Millipore Corp., Billerica, MA) and stainless steel screens with twill weave (SS635) were tested in this work (Table 3-1). Nylon 6-6 is a commonly used synthetic polymer composed of hexamethylene diamine and adipic acid that each contain 6 carbon atoms (hence 6-6). As shown in Figure 3-1, these mesh screens exhibit uniform openings with fibers arranged at 90-degree angles. The packing density (α) or solid volume fraction of the nylon screens was calculated as:

$$\alpha = \frac{4\, m_s}{\pi\, d_s^2\, h\, \rho_s}, \tag{3-1}$$

where m_s is the mass of the screen measured using a microbalance (Model AX504 Delta Range, Mettler-Toledo Inc., Columbus, OH), d_s is the diameter of the screen reported by the manufacturer, h is the thickness of the screen reported by the manufacturer and ρ_s is the density of the screen (1.15 g/cm^3 for nylon 6-6).

Experiments

Pressure Drop and Single-Fiber Efficiency

For each pore size, five screens were mounted in each of the ten stages of the diffusion battery (inner diameter, d_0=3.81 cm) of a Diffusional Particle Sizer System

(Model 3040, TSI Inc., Shoreview, MN). The pressure drop across all 50 screens was measured with an inclined manometer (Model 400, Dwyer Instruments, Michigan City, IN) as a function of superficial velocity (U_0). Superficial velocity was calculated as: $U_0 = Q / A_0$ where Q is the airflow rate through the diffusion battery screen and A_0 is the screen area calculated using d_0. Airflow rate was measured with a mass flowmeter (Model 4199, TSI Inc., Shoreview, MN) and varied from 1 Lpm (U_0 = 1 cm/sec) to 90 Lpm (U_0 = 130 cm/sec).

Using the same screen arrangement described above in the diffusion battery, particle collection efficiency by size was measured at flow rates of 2.5, 4 and 6 Lpm (Figure 3-2). Flow rates of 4 Lpm and 6 Lpm were selected to make this work directly comparable to that of Cheng et al. (1985), whereas the 2.5 Lpm flow rate was selected because it is a commonly used sampling flow rate for industrial hygiene equipment. Stainless steel screens were first tests in the experimental set up for direct comparison with the work of Chen et al. (1985). Nylon screens were subsequently mounted in the diffusion battery. Polydisperse ammonium fluorescein aerosol with a count median diameter of 60 nm and geometric standard deviation of 2.0 was generated by nebulizing a solution of 0.19% (by volume) fluorescein ($C_{20}H_{12}O_5$) in 0.01 N ammonium hydroxide with a six-jet collison-type nebulizer (BGI, Waltham, MA). This aerosol distribution was selected to cover the wide particle size range between 10 and 300 nm. Compressed air was filtered with a high-efficiency particulate air (HEPA) filter, controlled with a regulator and fed into the nebulizer. The polydisperse aerosol was passed through a diffusion dryer (Model 3062, TSI Inc., Shoreview, MN) and a charge neutralizer (Model 3054, TSI Inc., Shoreview, MN). A scanning mobility particle sizer (SMPS – Model 5.4, Grimm Technology, Douglasville, GA) was used to measure number concentrations by size entering Stage 0 of the diffusion battery (no screens, C_{in}) and exiting even stages between Stage 2 and Stage 10 (C_{out}) in the sequence: 0-2-0-4-0-6-0-8-0-10. After one sequence, new screens were placed in the diffusion battery and the measurements were

repeated to obtain a total of three replicates for each pore size and flow rate. The switching valve of the Diffusional Particle Sizer System was used to sequentially connect each exit port of the even stages of the diffusion battery to the SMPS.

Aerosol penetration (P) was calculated for SMPS midpoint diameters between 10 and 100 nm at 10 nm intervals, and 150, 200 and 300 nm as $P_{i,j,k} = C_{out,i,j,k} / C_{in,i,j,k}$, where i is the diffusion battery stage number (2 through 10), j is the SMPS midpoint diameter and k is the replicate (1 through 3). Following Cheng et al. (1985), the logarithm with base 10 of aerosol penetration by size was plotted relative to the total number of screens the aerosol passed in a corresponding stage i. Linear regression of the form $\log(P_{j,k}) = m_{j,k}\, n$, where n is the number of screens, was performed on the plotted data and single-fiber efficiency (η) by size was calculated from the slope (m) as:

$$\eta_{j,k} = -m_{j,k}\, ln10/B, \tag{3-2}$$

where $B = 4\alpha h/(\pi(1-\alpha)d_f)$ and d_f is the fiber diameter. Mean single-fiber efficiencies of the three replicates were then plotted as a function of particle diameter, compared to estimates from theory (Cheng et al., 1985), and assessed for fit.

Effect of Morphology on Collection Efficiency

The effect of morphology on the collection efficiency of nylon mesh screens was observed for highly fractal and spherical particles using the experimental setup shown in Figure 3-3. Following Ku and Maynard (2006), silver (Ag) particles of varying morphology were generated using two horizontal tube furnaces in series. The first furnace (Lindberg/Blue, Laboratory Tube Furnace STF55433C) was operated at 1200 ˚C with pure nitrogen (purity level 99.999%) at an airflow of 1.0 Lpm passed over silver wire (purity level 99.9%) placed in a ceramic boat. A digital mass flow controller (Model 0154, Brooks Instrument, Hatfield, PA) was used to maintain a constant nitrogen flow rate. The aerosol leaving the first furnace was passed through a coagulation chamber

(residence time ~ 40 sec) where the aerosol cooled to form chain agglomerates with an open structure (Figure 3-4, A). For highly fractal tests, the second furnace (Blue TF55035A, Blue M, New Columbia, PA) was operated at room temperature (furnace off). Alternatively for spherical particle tests, the second furnace was operated at 600 ˚C to sinter the agglomerates so that they would form spheres when cooled (Figure 3-4, B). The particles shown in Figures 3-4, A and 3-4, B were collected with an electrostatic precipitator located in place of the filter holder in the setup shown in Figure 3-3 and were analyzed under transmission electron microscopy. Filtered compressed air at 1.5 Lpm was added after the second furnace to bring the flow rate to the commonly used sampling flow rate for industrial hygiene equipment of 2.5 Lpm.

Collection efficiency was measured for screens with 60-µm pore size (NY60), at 2.5 Lpm, for 15, 40 and 100 nm mobility diameters, and for spherical and highly fractal particle morphologies. An electrostatic classifier (Model 3080L, TSI Inc., Shoreview, MN) was used to select the mobility diameters. A polonium-210 radioactive source (Model 2U500, NRD LLC, Grand Island, NY) was used to neutralize the aerosol before it was passed through a stack of either five NY60 screens (for the 20 nm tests) or twenty NY60 screens (for the 40 and 100 nm tests). New screens were passed under a polinium-210 source (Model 2U500, NDR LLC, Grand Island, NY) for 10 seconds and loaded in the filter holder before each test. A condensation particle counter (Model 3022A, TSI Inc, Shoreview, MN) was used to measure monodisperse aerosol concentration for 120 seconds before (C_{in}) and after (C_{out}) passing through the screens. This measurement procedure was repeated three times. Collection efficiency was calculated as E=1-(average C_{out} / average C_{in}), where the average represents the mean of the concentration over 120 seconds.

Modification of Theory

Single-fiber efficiency of screens can be expressed as the sum of the individual efficiencies for diffusion, interception and a correction term for diffusion and interception (Kirsch and Stechkina, 1978; Cheng et al., 1980 and 1985). Theoretical single-fiber efficiency of the nylon mesh screens was estimated following Cheng et al. (1985) as:

$$\eta = 2.7\, Pe^{-2/3} + 2\,(2\kappa)^{-1}\, R^2 + 1.24\, \kappa^{-1/2}\, Pe^{-1/2}\, R^{2/3}, \qquad (3\text{-}3)$$

where Pe is Peclet number ($Pe = d_f\, U_0\, /D$), $\kappa = -(1/2)\ln c - 0.75 + c - (c2/4)$, $c = 2\alpha\, /\pi$, R is the interception parameter ($R = d_p\, /d_f$), U_0 is the superficial velocity, and d_p is the particle diameter. D is the diffusion coefficient $D = k_B\, T\, Cc\, /6\, \pi\, \mu\, d_p$, where k_B is Boltzmann constant, T is temperature, Cc is the slip correction factor, and μ is the air viscosity. The coefficients of each term in Equation 3-3 were originally determined through laboratory experiments performed by Kirsch and Fuchs (1968).

The experimental single-fiber efficiency values for a given particle size, calculated using Equation 3-2, were used to modify the coefficients of each term in Equation 3-3 (2.7, 2, and 1.24). New coefficients were determined to minimize the sum of the square error (SSE) between theoretical and experimental single-fiber efficiency values. The solver function (MS Excel, Microsoft Corp., Redmond, WA) was used to minimize the SSE by iteratively changing the three coefficients in Equation 3-3.

Results and Discussion

Pressure Drop and Collection Efficiency

A linear relationship was observed between pressure drop and superficial velocity for all pore sizes over the velocity range from 1 to 130 cm/sec (Figure 3-5). A linear relationship between pressure drop and superficial velocity is an underlying assumption of a filtration theory for calculation of particle collection efficiency that is based on single-fiber efficiency (Cheng et al., 1985).

Mean experimental single-fiber efficiencies as a function of particle diameter with 95% confidence interval error bars are provided in Figure 3-6 (closed symbols) for NY60 screens at 6 Lpm. The theoretical expression of Equation 3-3 (solid line) is in good agreement with estimates of single-fiber efficiency for nylon net screens for particles between 40 and 150 nm, where theory was within the 95% confidence intervals of the experimental data points. Theoretical estimations, however, were outside of the 95% confidence intervals of the experimental data for particles smaller than 40 nm, where efficiency was overestimated, and larger than 150 nm, where efficiency was underestimated.

This work represents the first measurements of collection efficiency of nylon net screens for submicrometer particles. The theoretical estimations of the single-fiber efficiency model tested by Cheng et al. (1985) on stainless steel screens have been used to determine the number and pore size of nylon mesh screens for a size-selective collector for particles smaller than 0.25 μm (Gorbunov et al., 2009). The collection efficiency of nylon mesh screens, however, has only been investigated for micrometer-sized particles ranging between 0.3 to 100 μm (Yamamoto et al., 2005). In their work, Yamamoto et al. (2005) found high variability in experimental data and discrepancies between theoretical and experimental collection efficiencies. Particularly, they found that the theoretical estimations were higher than the experimental collection efficiencies for particles smaller than 5 μm and larger than 20 μm. The present tests and evaluations of collection efficiency for submicrometer particles, coupled with the analytical advantages of the nylon fibers, provide valuable information for future uses of nylon mesh screens as particle collection media.

Effect of Morphology on Collection Efficiency

The results of the silver particle morphology tests are summarized in Table 3-3. For each mobility size, morphology affected efficiency by less than 4%. No specific

morphology was found to affect overall efficiency more than another. For the 15-nm aerosol, highly fractal particles had smaller collection efficiency (34.3%) than spherical particles (37.9%). Conversely, for 40 and 100-nm mobility sizes the spherical particles had smaller collection efficiency (43.9% and 23.4% respectively) while highly fractal particles had larger collection efficiency (45.6% and 24.0% respectively).

Highly fractal particles have larger interception lengths than spherical particles; however, when compared to the screen fiber diameter (33 μm), the particles studied in these tests were so small (≤100 nm) that interception may not play a significant role in their collection. Visual comparison between fiber diameter and particle size can be observed in the inset in Figure 3-1, showing fluorescein nanoparticles deposited on a NY60-screen fiber. These efficiency similarities are consistent with the findings for fibrous filters of Kim et al. (2009), who found that for particles smaller than 100 nm penetration through filters was similar regardless of particle morphology.

These results have implications for the evaluation of theory. A significant effect of morphology on the screen's overall efficiency would have warranted the inclusion of this factor in the theoretical model. These tests confirmed the negligible effect of morphology on collection efficiency of submicrometer particles and validated its exclusion from theoretical estimation models.

Modification of Theory

The experimental collection efficiency data was used to empirically modify the coefficients of Equation 3-3. These coefficients were estimated by minimizing the SSE between theoretical and experimental data. The SSE values for the theoretical model with the original coefficient (Equation 3-3) and modified theory with new coefficients are reported in Table 3-2. The modified coefficients are 2.3, 2 and 4.3, thus the modified single-fiber efficiency theory is expressed as:

$$\eta = 2.3\, Pe^{-2/3} + 2\,(2\kappa)^{-1}\, R^2 + 4.3\, \kappa^{-1/2}\, Pe^{-1/2}\, R^{2/3}. \qquad (3\text{-}4)$$

For all screen types and flow rates tested, the SSE was lower for the theory with the modified coefficients than for that with the original coefficients (Table 3-2), indicating improved fit. The SSE was at least one order of magnitude lower when calculated using Equation 3-4 for all screens and flow rates with the exception of the NY60 screens at 2.5 Lpm flow rate, where the decrease was threefold.

The improved agreement between the modified single-fiber efficiency and the experimental data is visible in Figure 3-6, where the dotted line represents the modified theoretical estimations of Equation 3-4. Figure 3-7 presents mean experimental single-fiber efficiency and theoretical estimations calculated using Equation 3-4 for all pore sizes and flow rates tested, showing that the theoretical values estimated with the modified coefficients fall within the 95% confidence interval error bars of the experimental values. The new model (Equation 3-4) can therefore be used for estimating theoretical efficiency of nylon net screens if the physical dimensions of the screens (i.e., screen thickness, fiber diameter and packing density) are known as E=1-exp(-ηBn), where η is Equation 3-4 and n is the number of screens.

Estimates of single-fiber efficiency made with the original theory (Equation 3-3) fell within the 95% confidence interval of experimental data only for particles between 40 and 150 nm for both nylon and stainless steel screens. The tests performed with the stainless steel screens allowed direct comparison of our results with those of Cheng et al. (1985), who found that this model fit experimental values well for stainless steel screens for all particle sizes tested from 0.22 to 0.95 um. Deviation of experiment from theory was expected for nylon but not stainless steel screens.

The deviation observed for stainless steel screens may be due to differences between the experimental setup and the instrumentation used in this study and that of Cheng et al. (1985). Cheng and coworkers generated polydisperse oleic acid aerosol that was subsequently classified to yield monodisperse fractions. Aerosol concentrations were measured simultaneously with a condensation nucleus counter (CNC) and a Faraday cup

with an electrometer, and the slopes obtained from the linear regression on aerosol penetration by number of screens of the two sets of data were averaged prior to the calculation of single-fiber efficiency. This method yielded one single-fiber efficiency value per particle size and no indication of the variability within measurements for each particle size. In our experiments, we generated polydisperse ammonium fluorescein aerosol and measured aerosol concentration by size using an SMPS. This method greatly reduced the number of experiments and allowed us to obtain triplicate measurements for each particle size. Linear regression was performed on each set of data and the linear regression slopes were not averaged prior to the calculation of single-fiber efficiency. The single-fiber efficiency values obtained from the slopes were averaged and the repeated measurements were used to estimate 95% confidence intervals around the mean efficiencies.

A similar approach to developing empirical efficiency models has been taken by Wang et al. (2007). In a study that investigated the filtration efficiency due to diffusion of standard filters for particles ranging between 3 and 400 nm, they compared experimental data with a theoretical filtration model similar to the one used in this study. Wang et al. (2007) averaged the model coefficients obtained from experimental data of four filter medias to develop a new model that better estimates the filter's collection efficiency. Unlike nylon net screens, standard filters have non-homogeneous fiber diameters that make it difficult to theoretically express filtration efficiency.

There are some limitations to this work. The modified single-fiber efficiency model provided in this study (Equation 3-4) may not apply to particle sizes outside of the range observed in this study (10-300 nm). Additionally, nylon fibers may develop and retain static electricity charges that may affect the collection efficiency of the screens. The effect of these charges on particle collection efficiency was not investigated in this study. The effects of particle morphology were tested on silver particles; therefore, the results obtained may not apply to fibrous particles such as carbon nanotubes.

Conclusions

The pressure drop and submicrometer particle collection efficiency was measured experimentally for three pore sizes of nylon mesh screens. The effects of particle morphology on collection efficiency of the screens were also evaluated. No substantial effects on efficiency changes were found for spherical and highly fractal silver particles. Single-fiber efficiency of the nylon mesh screens was calculated from the experimental data and compared to the theoretical estimations for fibrous filters of Kirsch and Stechkina (1978) adapted for mesh screens by Cheng et al. (1980). The results of this comparison indicated that the theoretical estimations were in good agreement with the experimental data for particles between 40 and 150 nm, but the experimental data deviated from theory for particles smaller than 40 nm and larger than 150 nm. A modified theory to estimate collection efficiency of nylon mesh screens was generated by empirically modifying the model's coefficients. The modified theory was found to better match the experimental data and fell within the 95% confidence interval limits of the experimental data.

Nylon mesh screens provide a low-cost, disposable collection surface suitable for collection of nanoparticles and compatible with a wide range of analysis methods. The ability to accurately estimate collection efficiency of submicrometer particles and of analyzing their composition with minimal interference from the nylon fibers makes nylon mesh screens an ideal collection substrate for nanoparticles. The use of nylon mesh screens as diffusion material may help better understand and estimate workers' exposure to nanoparticles.

Table 3-1: Physical specifications of the nylon mesh screens.

Screen Model	Pore Size [µm]	Open Area [%]	Thickness, h [µm]	Fiber Diameter, d_f [µm]	Mass (StDev) [mg]	Packing Density, α
NY60	60	41	50	33	31.9 (0.5)*	0.32
NY1H	100	44	80	51	45.5 (0.2)*	0.29
NY8H	180	47	135	83	83.4 (0.3)**	0.31
SS635	~60	n/a	50†	20†	n/a	0.35†

* From Yamamoto et al. (2005)

** Weighed by microbalance (n=8)

† From Cheng et al. (1985)

Table 3-2: Sum of squares error between experimental single-fiber efficiency values and theoretical models (original and modified).

Screen Type	Flow Rate [Lpm]	Sum of Squares Error	
		Original Theory (Equation 3-3)	Modified Theory (Equation 3-4)
NY60	2.5	8.65×10^{-3}	2.43×10^{-3}
	4	3.08×10^{-3}	5.59×10^{-4}
	6	4.86×10^{-4}	3.83×10^{-5}
NY1H	2.5	9.50×10^{-4}	5.07×10^{-5}
	4	6.53×10^{-4}	5.57×10^{-5}
	6	1.77×10^{-4}	5.25×10^{-5}
NY8H	2.5	8.43×10^{-4}	5.87×10^{-5}
	4	4.41×10^{-4}	2.39×10^{-5}
	6	2.11×10^{-4}	4.46×10^{-6}
SS635	2.5	1.32×10^{-2}	3.76×10^{-3}
	4	2.95×10^{-3}	2.23×10^{-4}
	6	3.54×10^{-3}	8.58×10^{-4}

Table 3-3: Effects of particle morphology on collection efficiency of NY60 screens.

Particle Diameter [nm]	Number of Screens	Collection Efficiency (Standard Deviation) [%]	
		Spherical	Highly Fractal
15	5	37.9 (0.6)	34.3 (0.7)
40	20	43.9 (0.1)	45.6 (0.5)
100	20	23.4 (0.3)	24.0 (0.2)

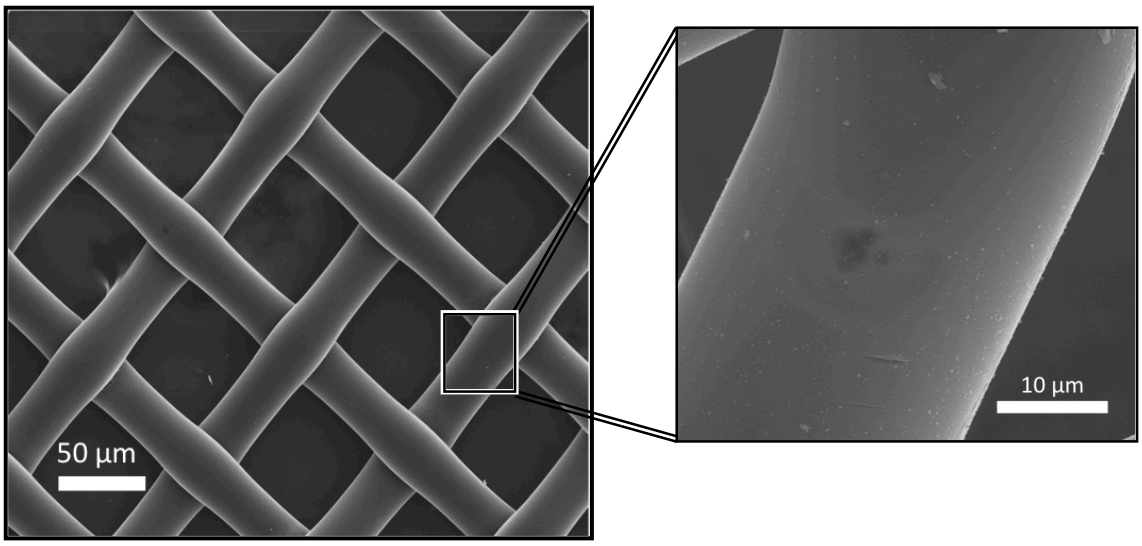

Figure 3-1: Scanning electron microscopy image of NY60 nylon mesh screen with insert showing fluorescein loading (white spots) on a single fiber.

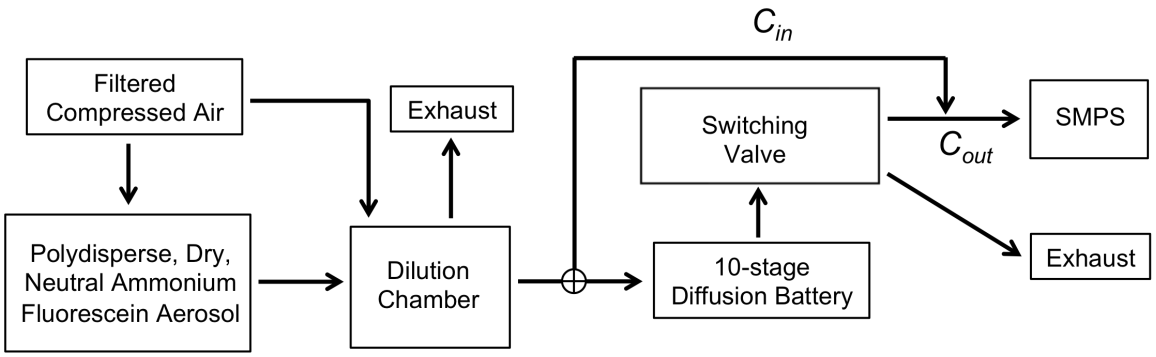

Figure 3-2: Experimental setup for submicrometer particles collection efficiency tests.

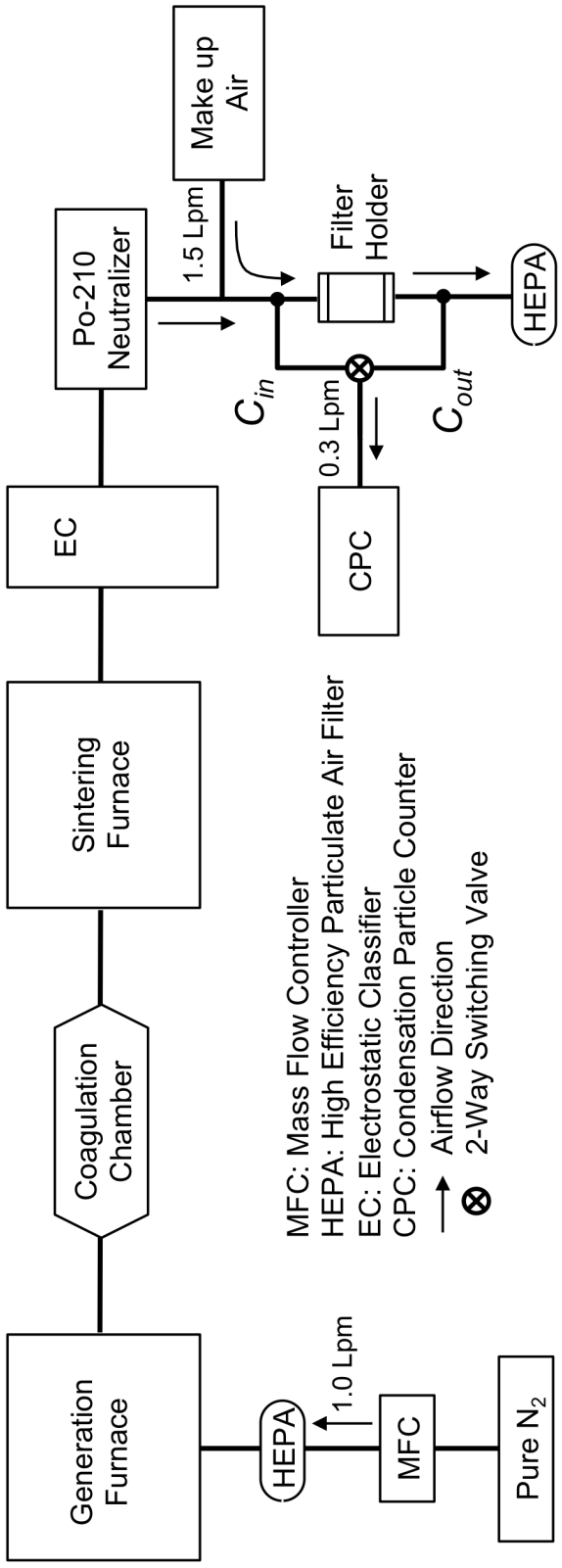

Figure 3-3: Experimental setup for evaluation of particle morphology on collection efficiency (adapted from Ku and Maynard, 2006).

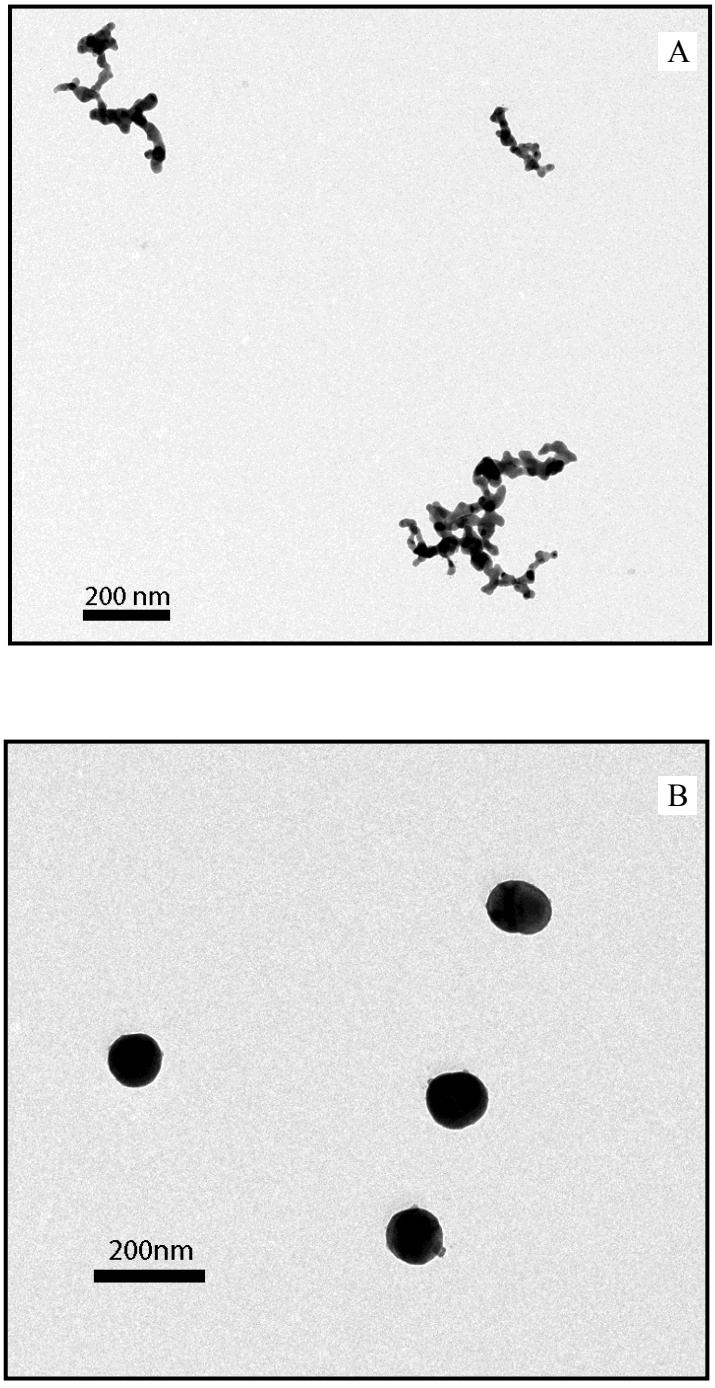

Figure 3-4: Transmission electron microscopy images of (A) highly fractal Ag nanoparticles (no sintering) and (B) spherical Ag nanoparticles (600 ˚C sintering).

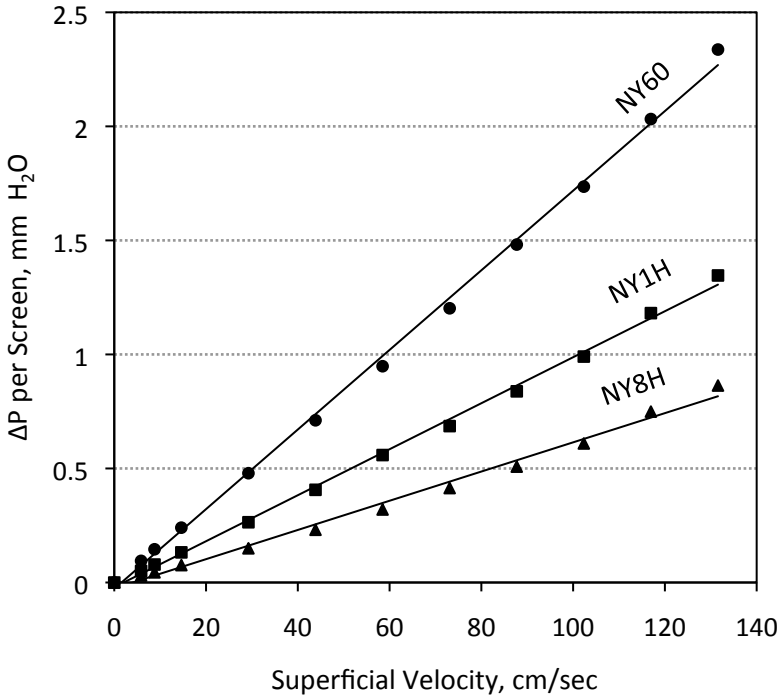

Figure 3-5: Pressure drop per screen as a function of superficial velocity.

Note: Solid line is a linear regression through data points.

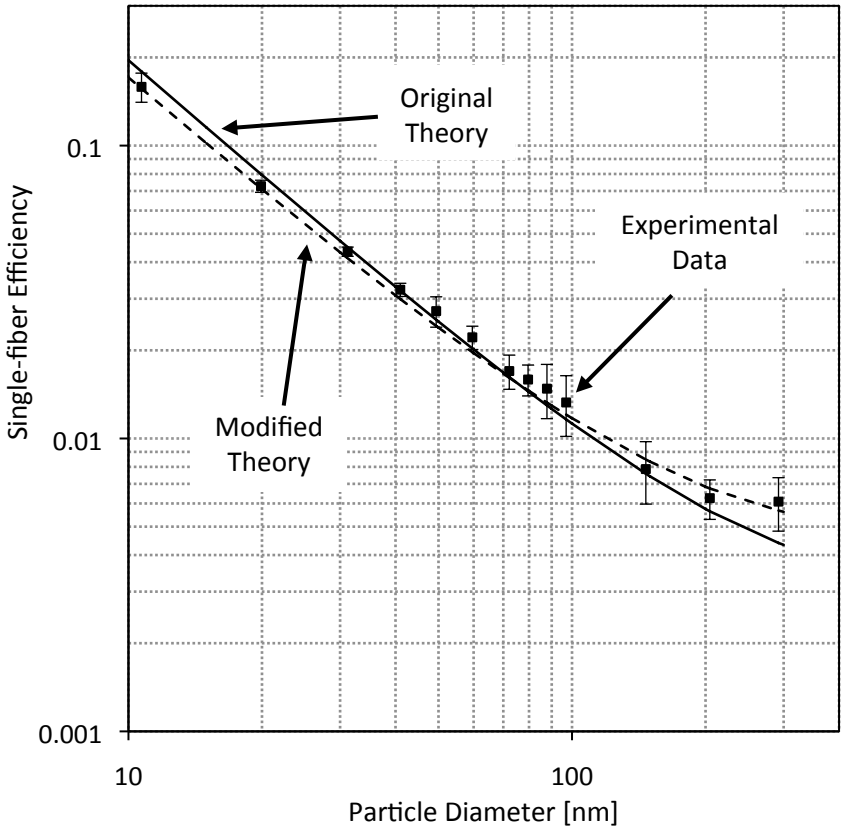

Figure 3-6: Experimental data with comparison of original and modified single-fiber efficiency theory for NY60 screens at 6 Lpm.

Note: Error bars represent 95% confidence intervals.

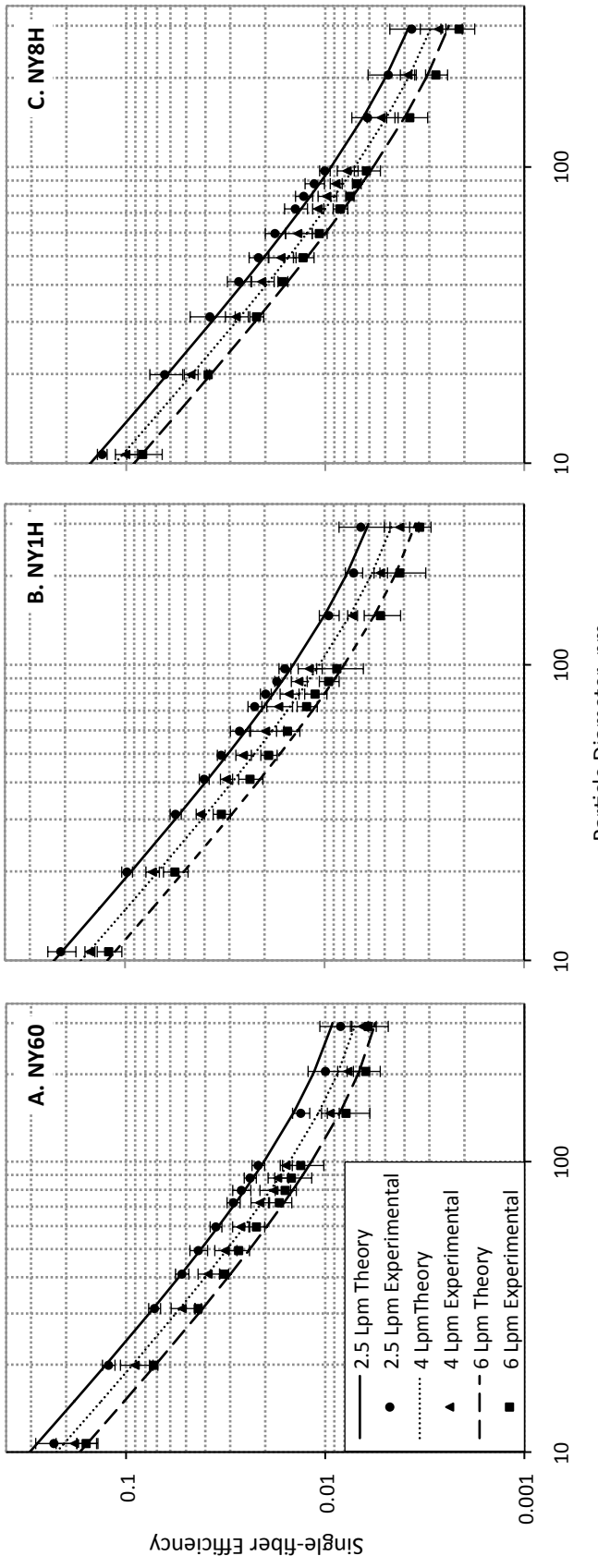

Figure 3-7: Theoretical (Equation 3-4) and experimental single-fiber efficiency of (A) NY60 screens, (B) NY1H screens and (C) NY8H screens.

Note: Error bars represent 95% confidence intervals.

CHAPTER IV

A PERSONAL NANOPARTICLE RESPIRATORY DEPOSITION (NRD) SAMPLER

Abstract

Nanoparticles can elicit substantially greater toxic effects than larger particles of the same composition. However, the mass of nanoparticles is often obscured by that of larger particles in samples collected with traditional 8-hr, filter-based personal samplers (e.g., respirable samplers). This work describes the development of a personal nanoparticle respiratory deposition (NRD) sampler that selectively collects particles smaller than 300 nm in the manner that they typically deposit in the respiratory system. A sampling criterion for nanoparticulate matter (NPM) was defined, using the International Commission on Radiological Protection deposition curve, to serve as a target for the development of the sampler. The NRD sampler consists of a respirable cyclone fitted with an impactor and a diffusion stage that contains eight nylon-mesh screens. The sampler operates at 2.5 Lpm and fits on a worker's lapel. The efficiency of the impactor was tested using sodium chloride aerosol with and without prior loading of the impaction plate to determine its ability to tolerate typical workplace loading without performance disruptions. The cut-point diameter of the impactor was 300 nm with a sharpness σ = 1.53. Loading at typical workplace levels was found to have no significant effect on the impactor's performance. The effective deposition of nanoparticles on the mesh screens of the diffusion stage with the respirable cyclone and impactor present was measured by depositing 20, 40, 100, 200 and 500 nm monodisperse ammonium fluorescein particles, which were subsequently recovered and measured with the use of a fluorometer. The effective deposition of the NRD sampler was found to match the NPM sampling criterion, showing that a sample collected with the NRD represents the concentration of

nanoparticles deposited in the human respiratory system. The sampler can also be easily modified to match alternative future collection criteria for nanoparticles.

Introduction

Workers produce and handle engineered nanomaterials in substantial quantities in the manufacture of hundreds of commercial products (Hansen et al., 2008). Exposure through inhalation of these materials is a primary concern for worker health and safety because of the sensitivity of the respiratory system (Papp et al., 2008). The airborne nanoparticle component (≤ 100 nm) is of particular concern because nanoparticles can elicit substantially greater toxic effects than larger particles of the same composition (Oberdörster et al., 1994; Grassian et al., 2007). Moreover, nanoparticles may translocate from the respiratory tract to other organs and the blood stream (Oberdörster et al., 2002 and 2004). The National Institute for Occupational Safety and Health (NIOSH) has proposed draft guidelines for ultrafine titanium dioxide, which includes recommended exposure limits and exposure assessment method (NIOSH, 2005b). The proposed exposure assessment method relies on traditional 8-hr, filter-based, personal respirable sampling (NIOSH, 2005b).

Size-selective samplers are used to collect particles with efficiencies that represent how particles enter into or deposit within the respirator system. Respirable samplers are used to collect particles with efficiencies that approximate the fraction of aerosol that, once inhaled, can penetrate into the gas-exchange region of the respiratory tract (Vincent, 1999). They are designed to match a specific sampling criterion, which defines collection efficiency of particles to the filter as 50% for 4-μm particles and 100% for particles smaller than 1 μm (ACGIH, 2010). By this definition, respirable samplers must prevent the collection of larger particles (>10 um) that may exist in the environment while selectively sampling only these smaller particles at the specified collection efficiencies. However, when aerosols include both nanoparticles and respirable particles,

the mass measured from a sample collected using a respirable sampler will be dominated by the larger, non-nanoparticles. Hence, in many occupational environments where both nanoparticles and respirable particles coexist, the respirable sampler has limited usefulness in quantifying nanoparticle exposures.

To overcome this problem for assessing titanium dioxide nanoparticle exposures, NIOSH recommends both mass-based respirable sampling analysis coupled with analysis by electron microscopy (NIOSH, 2005b), where the nanoparticles would be characterized with an energy dispersive x-ray analyzer. However, there are no standard methods for this analysis, and electron microscopy is particularly expensive (>$300 per sample) compared to bulk analysis methods (~$30 per sample). A personal sampling method that removes larger particles and only collects nanoparticles would streamline exposure assessment.

Wire mesh screens have been used successfully to preferentially collect nanoparticles (Yeh et al., 1982). The Brownian motion of particles smaller than 300 nm enhances their deposition onto the surface of the wires by diffusion (Kleinstreuer et al., 2008). Stainless steel screens have typically been used, although they are incompatible with bulk analyses techniques that require dissolution of the collection media (Grohse, 1999). Gorbunov et al. (2009) developed a size-selective sampler that uses an impactor to remove large particles and nylon mesh screens to collect nanoparticles. They analyzed these nanoparticles by treating the nylon mesh screens in *aqua regia* and subjecting them to microwave digestion. While it provides a method for separating and analyzing nanoparticles from other aerosol components, its large size limits this sampler to area sampling and does not collect particles with physiological relevance.

Because exposure assessors have a need to characterize exposures to nanoparticles in environments where other size-fractions may exist, a need exists to develop a sampler that can preferentially eliminate large particles and allow quantification of small, nanoparticle aerosols. An ideal sampler would be portable, allow

placement within the breathing zone of a worker and collect nanoparticles in a way that mimics their respiratory deposition (Johnson and Esmen, 2004). By capturing only nanoparticles on the sampling media, cost-efficient bulk analysis techniques could then be used to estimate the amount of deposited nanomaterials.

This work presents the development of a personal nanoparticle respiratory deposition (NRD) sampler capable for deployment as a full-shift, personal sampler that selectively collects nanoparticles apart from larger particles in a workplace atmosphere. Rather than attempting to collect nanoparticles with 100% efficiency, the sampler was designed to collect nanoparticles as they deposit in the respiratory tract to provide a physiologic relevance to sampler's performance. Consequently, the NRD sampler is fundamentally different from commonly used samplers (e.g., respirable and inhalable samplers) that are based on penetration of particles to different regions of the respiratory system (Soderholm and McCawley, 1990). A new sampling criterion—nanoparticulate matter (NPM)—was first devised to provide the target collection efficiency, by particle size, for the sampler. The NRD sampler presented here was developed by incorporating a respirable sampler (to eliminate particles larger than 10 um), an impaction plate (to further remove particles down to 300 nm) and a deposition stage where the remaining nanoparticles deposit onto nylon mesh screens with collection efficiency to match this target sampling criterion. Subsequent chemical analysis of the nanoparticles deposited on the collection media of the NRD sampler allows for characterization of nanoparticles apart from larger background particles.

Methods

Development of a Target Size Selection Curve

Particle deposition in all regions of the respiratory tract is shown as the dashed line in Figure 4-1. Deposition of particles measured experimentally under a wide variety

of conditions (Heyder et al., 1986; Kim and Hu, 1998; Kim and Jaques, 2000) generally follows the respiratory deposition curve for the average adult under light exercise and nose-breathing conditions presented by the International Commission on Radiological Protection (ICRP, 1994). For this reason, the ICRP curve was used to develop the NPM sampling criterion. The region of interest for the NPM curve was all particles smaller than 300 nm, the minimum deposition for sub-micrometer particles.

We have defined NPM fraction, for a given particle size, as the fraction of those particles that, when inhaled, can deposit in the respiratory system. Therefore, the NPM fraction is a subset of the inhalable particulate matter (IPM) collection efficiency, defined as:

$$\mathrm{IPM}(d)=0.5[1+\exp(-0.06\,d)] \text{ for } (0 < d \leq 100\ \mu\mathrm{m}), \tag{4-1}$$

where d is the particle diameter in μm (ACGIH, 2010). The collection efficiency for NPM is, therefore, given by:

$$\mathrm{NPM}(d)=\mathrm{IPM}(d)[1-\mathrm{F}(x)], \tag{4-2}$$

where $\mathrm{F}(x)$ is the cumulative probability density function of the standardized normal variable x,

$$x = \frac{\ln(d/\Gamma)}{\ln(\Sigma)}, \tag{4-3}$$

with $\Gamma = 0.04$ μm (40 nm), and $\Sigma = 3.9$. The mathematical form for this criterion is the same as that used for the thoracic and respirable criteria (ACGIH, 2010). The value for Γ represents the particle size associated with 50% deposition, or d_{50} cutoff diameter. This value was selected as the particle size smaller than 300 nm associated with 50% deposition as defined by the ICRP curve. Examining Figure 4-1, we find that in this region $d_{50} = 40$ nm. The value for Σ was fitted by minimizing the sum of squares error between the ICRP total deposition curve and the NPM equation for particles smaller than

300 nm. This minimization was carried out in a MS Excel (Microsoft Corp., Redmond, WA) spreadsheet using the solver function.

The resulting NPM sampling criterion is shown by the solid line in Figure 4-1. This criterion provided a rational target for the development of the NRD sampler and ties its performance to the physiologically relevant fractional deposition of nanoparticles in all regions of the respiratory tract. The shallow shape of the collection efficiency curve matched the collection efficiency performance form associated with diffusion techniques (rather than the sharp curve associated with impaction). This allowed the design of the sampler with diffusion screens to collect nanoparticles, achieving a sampler pressure drop small enough for use with conventional occupational hygiene belt-mounted sampling pumps.

Description of the NRD Sampler

The NRD sampler consists of three primary components assembled in series: a 25-mm respirable aluminum cyclone (Model 225-01-01, SKC Inc., Eighty Four, PA), an impaction stage and a diffusion stage (Figure 4-2). Air is drawn through the cyclone, which removes particles larger than the respirable sampler criterion and transports the respirable fraction to the impaction stage, where particles larger than 300 nm are removed. In the diffusion stage, the remaining airborne nanoparticles diffuse to and are collected onto a stack of eight hydrophilic nylon mesh screens with 11 μm pore size and 6% porosity (Model NY1102500, Millipore Inc., Billerica, MA) with an efficiency closely matching the NPM sampling criterion.

The sampler is lightweight (~60 g), fits in a standard lapel mount (Model 225-1, SKC Inc., Eighty Four, PA) and operates at an airflow rate (Q) of 2.5 Lpm with a pressure drop of 3.54 kPa (14.2 in. H_2O). The sampler can be used with a commercially available belt-mounted sampling pump for the duration of a work-shift (e.g., AirCheck 2000, SKC Inc., Eighty Four, PA).

The impaction stage was designed following Marple and Willeke (1976) impactor design procedures to achieve a d_{50} of approximately 300 nm at a flow rate Q = 2.5 Lpm. The initial design parameters included the selection of jet width (W) and number (n) to achieve a Reynolds number $500 < Re < 3000$. This stage consists of three round acceleration nozzles having a width W and throat length L, and an impaction plate at a distance S from the nozzles. The impaction plate requires the application of a thin layer of vacuum grease prior to operation. A description of the pilot designs of the impaction stage can be found in Appendix A. The final design parameters are presented in Table 4-1 and were calculated assuming temperature T = 20 ˚C, pressure P = 98.6 kPa, particle density ρ_p = 1000 kg/m^3, air density ρ_g = 1.2 kg/m^3 and air viscosity $\mu = 1.81\times10^{-5}$ Pa s.

Filtration theory from Cheng et al. (1985), validated and modified for use with nylon mesh screens in our previous work (Chapter III), was used to determine the number and mesh size of diffusion screens necessary to match the NPM sampling criterion. The diffusion screens are tightly held in place in the diffusion stage by an aluminum ring with three spokes.

Tests of the collection efficiencies of the impactor, both clean and pre-loaded, and the mesh screen diffusion collector were performed in series.

Evaluation of the Impactor Performance

The experimental setup shown in Figure 4-3 was used to evaluate the impaction stage. A three-jet Collison nebulizer (BGI, Waltham, MA) was used to aerosolize a 16% (by volume) aqueous sodium chloride (Fisher Scientific, Lot No. 028258) solution. The resulting polydisperse aerosol was fed into a dilution chamber, mixed with clean, dry air, and passed through a charge neutralizer (Model 3054, TSI Inc., Shoreview, MN) and a diffusion dryer (Model 3062, TSI Inc., Shoreview, MN). The aerosol was then passed into a 0.002 m^3 glass chamber, through the impactor stage and into a second identical glass chamber.

The particle number concentration by size was measured alternately from within the glass chamber upstream (C_{in}) and from within that downstream (C_{out}) of the impactor. A scanning mobility particle sizer (SMPS – Model 3080, TSI Inc., Shoreview, MN; airflow = 0.3 Lpm) was used to count particles from 15 to 500 nm, and an aerodynamic particle sizer (APS – Model 3321, TSI Inc. Shoreview, MN) was used to count particles from 0.5 to 2 μm. The APS was modified so that the sample entered directly into the aerosol inlet at 1 Lpm. A mass flow controller (Model GFC37, Aalborg Instruments & Controls Inc., New York, NY) was used to maintain a constant flow rate of 2.5 Lpm drawn through the impactor with a vacuum pump (Model 4F740A, Gast Manufacturing Inc., Benton Harbor, MI). The alternating of measurements upstream and downstream of the impactor was repeated at least three times. A differential pressure gauge (Magnehelic 2020, Dwyer Instruments Inc., Michigan City, IN) was connected to each glass chamber to measure the pressure drop across the impactor stage.

The collection efficiency (E) of the impactor stage for a given particle size (i) was calculated as: $E_i = 1 - C_{out,i} / C_{in,i}$. The collection efficiency data were fitted with a logistic sigmoidal algorithm (OriginPro v8.5, OriginLab Corporation, Northampton, MA) of the form

$$E = a_2 + \frac{a_1 - a_2}{1 + \left(\frac{d}{x_0}\right)^p}, \tag{4-4}$$

where a_1, a_2, x_0 and p are the coefficients determined by the algorithm. The sigmoidal algorithm allowed accurate estimation of the d_{50}, d_{84} and d_{16} of the impactor stage, which correspond respectively with the 50%, 84% and 16% collection efficiencies of the impactor. The sharpness (σ) of the collection efficiency curve was calculated as:

$$\sigma = \sqrt{\frac{d_{84}}{d_{16}}} \tag{4-5}$$

Evaluation of Impactor Performance after Loading

The performance of the impactor after being loaded with particles was evaluated using the experimental setup shown in Figure 4-4. An aerosol composed of fine test dust (Batch #1569, AC Spark Plug Company, Flint, MI) with 10-µm volume median diameter was generated using a fluidized bed aerosol generator (Model 3400, TSI Inc., Shoreview, MN) and injected into a 0.02 m^3 sampling chamber. The aerosol in the chamber was sampled simultaneously with two samplers: 1) the NRD respirable cyclone with the impactor stage downstream; and 2) the NRD respirable cyclone with a 37-mm filter cassette containing a Teflo filter (P/N 225-1709, SKC, Inc., Eighty Four, PA) with a support pad downstream. The filter was weighed before and after each test using a microbalance (Model MT5, ISO 9001, Mettler-Toledo Inc., Columbus, OH) to determine the mass concentration of dust passing to the impactor.

Two loading levels were targeted to simulate sampling in an environment with 3 mg/m^3 passing the cyclone to the impactor for 4 hrs (12 $mg/m^3 \times hr$) and 8 hrs (24 $mg/m^3 \times hr$). These values represent worst-case loading of the impactor at the threshold limit value established by the American Conference of Governmental Industrial Hygienists for respirable particles not otherwise specified over times relevant to workplace sampling. Actual loadings measured from the filter sampler for the 4 and 8 hrs loading scenarios were respectively 13.6 $mg/m^3 \times hr$, and 21.5 $mg/m^3 \times hr$.

After loading, the impaction stage was separated from the cyclone and placed in the previously described impaction stage evaluation setup (Figure 4-3). The sampler, now with pre-loaded impaction stages, was again tested with sodium chloride aerosol. The collection efficiency was measured in triplicate following the same procedures outlined above in the impaction stage evaluation. Two replicates of loading followed by collection efficiency measurement were performed for both loading levels. The impaction substrate was cleaned and new grease was applied prior to each loading replicate measure.

Two-way analysis of variance (ANOVA) was performed (Minitab, Minitab Inc., State College, PA) on efficiency versus loading and particle size to determine whether the collection efficiency was significantly affected by loading of the impaction substrate ($p \leq 0.05$). The loading levels used in the ANOVA were no previous loading, 13.6 mg/m^3×hr, and 21.5 mg/m^3×hr.

Effective Deposition to the Screens of the NRD Sampler

The experimental setup presented in Figure 4-5 was used to measure the effective deposition on the diffusion stage of the NRD sampler. Deposition was computed for monodispersed aerosols with mean particle diameters of 20, 40, 100, 200 and 500 nm. To generate seed aerosol for 20-nm tests, an electrospray aerosol generator (Model 3480, TSI Inc, Shoreview, MN) was used to aerosolize a 0.01% (by volume) solution of ammonium fluorescein ($C_{20}H_{12}O_5$, Acros Organics, Lot No. A0206621001) in 0.01 N ammonium hydroxide (NH_4OH). A three-jet collison-type nebulizer (BGI, Waltham, MA) was used to nebulize an ammonium fluorescein solution of 0.03% by volume for the 40, 100 and 200-nm tests and 0.15% by volume for the 500-nm tests. The aerosol was fed into a dilution chamber, mixed with clean dry air and passed through an electrostatic classifier (Model 3071, TSI Inc., Shoreview, MN). Because of the difficulty to produce substantial concentrations of small (20 nm) fluorescein particles, the dilution chamber was removed during the generation of the 20-nm aerosol with the electrospray aerosol generator. The resulting monodisperse aerosol was neutralized (Model 3054, TSI Inc., Shoreview, MN) and dried (Model 3062, TSI Inc., Shoreview, MN) before entering a 0.02 m^3 sampling chamber. An SMPS (Model 5.4 Grimm Technology, Douglasville, GA) was used to verify particle size and number concentration in the sampling chamber.

The fully assembled NRD sampler (25-mm aluminum cyclone with impaction stage and diffusion stage containing 8 nylon mesh screens) and a 37-mm open-face filter cassette containing two Durapore membrane filters with a support pad (P/N DVPP04700,

Millipore, Billerica, MA) were placed inside the sampling chamber. Two separate vacuum pumps (Omni-5, BGI, Waltham, MA) were used to draw an airflow of 2.5 Lpm through each sampler. The vacuum pumps were calibrated with a mass flow meter (Model 4146, TSI Inc., Shoreview, MN) prior to each test. Particles were collected for a period of time ranging between 75 min for the 500 nm particles and 12 hrs for the 20 nm particles to ensure collection of a sufficient quantity of fluorescent material to detect particles on the collection substrate of the diffusion stage.

The amount of fluorescent material deposited on the screens of the diffusion stage and on the filter of the open-face cassette was determined following the protocol outlined by Tolocka et al. (2001). Both substrates were immersed in 4 ml of 0.01 N NH_4OH and sonicated (Solid State/Ultrasonic FS-14, Fisher Scientific Inc., Pittsburgh, PA) for 10 min. The mass concentration of fluorometric material in the recovered solution was determined using a fluorometer (Modulus 9200, Turner BioSystems, Sunnyvale, CA). The deposition efficiency (D_D) of particles on the diffusion stage was calculated as $D_D=M_D/M_F$, where M_D is the mass concentration of fluorometric material deposited on the diffusion substrate and M_F is that deposited on the filter of the open-face cassette. These deposition and recovery procedures were repeated three times for each particle size, and new nylon mesh screens and filters were used for each repetition. Mean deposition efficiency of these repetitions was compared to the NPM curve and assessed for fit.

Results and Discussion

Evaluation of the Impactor Performance

The results of the collection efficiency tests performed with the pilot designs of the impactor are reported in Appendix A.

The collection efficiency curve of the impaction stage is shown in Figure 4-6, and the physical characteristics and parameters of the stage are reported in Table 4-1. The minimum collection efficiency (8% ± 3%) was observed for particles with a diameter near 100 nm. For particles progressively smaller than this minimum value, collection efficiency gradually increased to 26% (± 7%) for 15 nm particles. This increase in efficiency is attributed to diffusion losses that may occur throughout the impactor stage. A similar increase in efficiency due to diffusion was observed in the smallest stages of a recently developed, high flow rate (40 Lpm), portable nanosampler consisting of four impaction stages and an impaction filter (Furuuchi et al., 2010). For particles larger than 100 nm, the collection efficiency of the NRD sampler impaction stage rapidly increased to 96% (± 6%) for 550 nm particles. Particles in this size range carry sufficient inertia to impact upon the greased impaction plate where they were trapped.

The characteristic cut-off diameter (d_{50}) of the impactor stage was measured to be 295 nm, and the geometric standard deviation (σ) or collection efficiency sharpness was 1.53. This curve is sufficiently sharp to remove particles larger than the target cutoff diameter (300 nm) from the airstream. The square root of Stokes number at the 50% collection efficiency was 0.32 and the pressure drop (ΔP) across the stage was 2.49 kPa. The Reynolds number of the impactor nozzles was 2,212, within the desired range of $500 < Re < 3000$, where the efficiency curve is at its sharpest (Marple et al., 2001).

Impactors have been developed that offer cut-off diameters similar to that of the NRD impaction stage (Hering et al., 1978; Hering and Marple, 1986; Hillamo and Kauppinene, 1991; Marple et al., 1991). For example, low pressure impactors operate at pressures substantially lower than atmospheric to reduce drag forces and allow collection of particles as small as 50 nm (Hering et al., 1979). Micro orifice impactors employ up to a few thousand small (40-200 μm) round nozzles to achieve smaller cutoff diameters. These impactors achieve sharper collection efficiency curves ($\sigma = 1.2$) than the impaction stage of the NRD sampler, however, they require rather large pumps to achieve high flow

rates and low pressures, making them less portable (Marple et al., 2001). In contrast, commercially available belt-mounted pumps are capable of handling the pressure drop imparted by the impaction stage of the NRD sampler.

Misra et al., (2002) developed a personal cascade impactor sampler that consists of four impaction stages and operates at a flow rate of 9 Lpm with a pressure drop of 2.7 kPa (11 in. of H_2O), a pressure drop compatible with a somewhat larger than normal belt-mounted vacuum pump. Similarly to the NRD impaction stage, the final stage of the personal cascade impactor achieves a cutoff diameter of 250 nm with collection efficiency sharpness ranging between 1.28 and 1.53 depending on the collection substrate employed in the stage (Misra et al., 2002).

Evaluation of Impactor Performance after Loading

The results of the loading tests performed on the impaction stage are summarized in Table 4-2. When compared to tests with no prior loading, the effect of particle loading on collection efficiency was negligible, as the mean ± one standard deviation overlap for all values in Table 4-2. The results of the two-way ANOVA confirmed that there is not a significant difference in efficiency between loadings (p-value = 0.257). The p-value for the interaction term between particle size and loading was close to significant (p-value = 0.063) at a 5% alpha level, indicating that with different loadings the efficiency varies at different particle sizes. The greatest reduction of the impactor's collection efficiency was observed at 15 nm, the smallest particle size tested, where efficiency after loading experienced the greatest decrease from $E = 0.26$ without prior loading to $E = 0.11$ after 13.6 mg/m^3×hr loading. This reduction is attributed primarily to greater uncertainty in this size channel because of lower particle counts. One-way ANOVA was performed on efficiency at the three loading levels for the 15 nm particles showing no significant difference (p-value = 0.102).

Loading of particles on the impactor plate yielded minimal effects (4% to 6% difference) at the largest particle diameters (>300 nm), where particle bounce had greater potential to affect the performance of the subsequent diffusion stage in the NRD sampler. Bounce of particles larger than 300 nm from the impaction plate would cause particles with substantially greater mass than nanoparticles to pass through the impactor and collect on the diffusion screens. This phenomenon would results in a positive sampling bias. The cut-off diameter of the impactor was not substantially shifted after loading (d_{50} = 265 nm for 13.6 mg/m^3×hr loading and 275 nm for 21.5 mg/m^3×hr loading). The test dust used in the loading tests contained considerable mass (10 µm volume median diameter) above the d_{50} of the cyclone of 4 µm, which passed through the cyclone and contributed to the loading of the impaction plate. This indicates that the impaction substrate can handle worst-case particle loadings without experiencing substantial shifts in the way that the impactor performs.

Lee et al. (2005) evaluated the performance of a greased metal plate in a single-stage, single-orifice impactor by loading up to 17 mg/m^3×hr polydisperse glass beads. They observed that at this loading there was minimum particle bounce and re-entrainment. The collection efficiency for particles larger than d_{50} remained high (95%) and constant, however, the collection efficiency curve was shifted and the d_{50} decreased from 5.26 to 4.36 µm. The discrepancy in the results of Lee et al. (2005) and the ones of the present study may be due to several factors. The acceleration nozzle of the single-stage impactor was rectangular (W = 0.15 cm and L = 5.59 cm), with a substantially larger cutpoint (5.26 µm) than the impactor developed for the NRD sampler. Additionally, the loading tests of Lee et al. were performed with glass spheres with size ranging between 3 and 10 µm, very different from the irregular surfaces of the dust particles used in this study's loading tests. Particles with uneven surfaces may experience increased adhesion to the greased impaction surface, making them less prone than spheres to the formation of a cone in the center of the impaction plate. The formation of a

cone of deposited particles on the impaction surface has been found to shift the efficiency curve to smaller diameter particles (Vanderpool et al., 2001; Peters et al., 2009b). Visual inspection confirmed the absence of these cones after the loading tests performed on the impaction plate of the NRD sampler.

Effective Deposition to the Screens of the NRD Sampler

The direct measurement of effective deposition of particles to the eight screens of the NRD sampler is shown in Figure 4-7 (open symbols). Deposition was lowest (6% ± 2%) for 500 nm particles, where the impactor efficiency was at its maximum, and gradually increased with decreasing particle size. This figure shows that the deposition to the screens was in agreement with the NPM sampling criterion (solid line), within uncertainty, for all points with the exception of the 200 and 500 nm particles where it matched within < 4%. This means that particles deposited on the screens can be analyzed to determine the concentration of nanoparticles that would deposit in the respiratory system.

Few examples of samplers with efficiencies matching respiratory deposition can be found in the literature. Of note is the size-selective inlet designed to mimic a modified ICRP lung deposition fraction for particles smaller than 1 μm developed by Kuo et al. (2005). The inlet was designed to remove large (> 1μm) and small (< 0.02 μm) particles and produce a resulting aerosol that simulates only the fraction *reaching* the ciliated regions of the lungs. No collection substrate following the inlet was developed, and rationale for the target curve that they used was not provided. Koehler et al. (2009) used polyurethane foam (PUF) as a selector and collector for particles to mimic total aerosol deposition in the respiratory tract. This PUF sampler follows the ICRP total respiratory deposition model. The PUF sampler provides a more physiologically relevant estimate of aerosol hazard than samplers that estimate aerosol aspiration fractions (Koehler et al., 2009), however, it is not specific to nanoparticles.

The NRD sampler presents an advantage over samplers traditionally used to collect particles in workplaces. Inhalable, thoracic and respirable particulate matter samples are designed to collect particulate matter that penetrates to a specific region of the respiratory tract (Soderholm and McCawley, 1990). These samplers overestimate the dose of particulate matter deposited in the respiratory tract because not all particles deposit (Koehler et al., 2009). In contrast, particles collected to the deposition stage of the NRD sampler represent the fraction of particulate matter smaller than 300 nm that deposits in the respiratory system. This deposited fraction provides a more reliable dose estimate and may better reflect adverse health effects related to aerosol inhalation (Esmen et al., 2002). This is particularly true for particles smaller than 300 nm as their deposition can occur anywhere in the respiratory tract (ICRP, 1994).

The NRD sampler can be modified in the future to follow a different deposition curve, should a different international standard ultimately be adopted. The impaction stage can be modified (using impaction theory) to adjust for the size fraction penetrating into the diffusion stage, and the number and mesh size of the screens in the diffusion stage can be modified (using filtration theory) to match a different deposition curve. Unlike respirable and inhalable particles, there is currently no available consensus on a sampling criterion for nanoparticles. In the absence of a consensus, the NPM criterion was developed as target efficiency for the NRD sampler, following the best available deposition curve for nanoparticles in the respiratory tract and agreeing with experimental lung deposition studies.

Conclusions

A nano-particulate matter (NPM) sampling criterion was developed as a target curve for a lightweight, personal nanoparticle respiratory deposition (NRD) sampler. The mathematical form of the NPM criterion is analogous to other size-selective occupational sampling criteria. However, this criterion specifies that sampler performance matches the

deposition of particles throughout the respiratory tract, unlike other criteria that are based on penetration of particles into specific respiratory regions (e.g., respirable and thoracic). It provides a rationale target for the development of samplers specific for assessing nanoparticle exposures.

The NRD sampler combines a commercially available respirable cyclone with a custom impactor and a diffusion stage, where nanoparticles deposit for traditional post-sampling analyses. The impactor demonstrated the desired cut-off diameter of 300 nm and was able to maintain desirable performance despite worst-case, heavy particle loading. The effective deposition efficiency to the screens of the NRD sampler was found in good agreement with the proposed NPM criterion. The NRD sampler is lightweight, portable and compatible with current occupational hygiene sampling techniques. It can easily be deployed in occupational settings as a personal sampler, and its use can be easily integrated into exposure assessment strategies and incorporated into epidemiological and toxicological studies where pure nanoparticle or mixed nanoparticle/respirable/inhalable aerosols exist.

The NRD sampler has some limitations that constrain its intended use to the estimation of personal exposure to airborne metal and metal-oxide nanoparticles. Sections of the nylon mesh screens can be analyzed with scanning electron microscopes for sizing, counting and assessing chemical composition of the particles collected on the nylon fibers, however, a comprehensive analysis of the particulate collected with the NRD sampler requires digestion of the nylon media and recovery of the particles. This digestion process limits the composition of the particles that can be recovered to metal and metal-oxide particles. Existing NIOSH methods (e.g., NMAM 7303) used to determine metallic content of respirable samples could be applied to the recovery of metallic particles from the nylon mesh screens followed by analysis using inductively coupled plasma mass-spectrometry. Based on this limitation, a practical application of the

NRD sampler may be the determination of the nanoparticulate component of personal exposures to welding fumes.

The collection efficiency of the NRD sampler is most accurate with spherical particles. The NRD sampler was tested with spherical particles and its behavior in the presence of fibrous particles such as carbon nanotubes is unknown. Fibrous particles may remain trapped in the impaction stage and depending on their orientation in the airstream their deposition on the diffusion stage of the NRD sampler may not reflect the NPM criterion for deposition in the respiratory tract.

Future work will include field tests of the NRD sampler and the development of analysis techniques to distinguish nanoparticles apart from background aerosols. These tests will be designed to provide information on the limit of detection of the analytical techniques to determine the duration of the sample collection. If sample collections longer than typical work-shifts are required, it will be necessary to determine how often the impaction plate requires cleaning and application of grease. Other practical aspects may also require investigation, such as the effects of tipping the sampler with the resulting drop of the particles collected in the cyclone's grid pot into the impactor.

Table 4-1: Physical characteristics, flow parameters and experimental results of the impaction stage.

Physical Characteristics			**Flow Parameters**		**Experimental Results**			
W **[cm]**	***L*** **[cm]**	***S/W***	***Re***	***V*** **[cm/sec]**	d_{50} **[µm]**	$\sqrt{Stk_{50}}$	Σ	ΔP **[kPa]**
0.053	0.135	1.9	2212	6295	0.295	0.32	1.53	2.49

Note: *W*, nozzle width; *L*, nozzle lengths; *S*, impaction plate-to-nozzle distance; *Re*, Reynolds number; *V*, nozzle air velocity; d_{50}, 50% cutpoint; $\sqrt{Stk_{50}}$, square root of Stokes number at 50% collection efficiency; σ, collection efficiency curve sharpness; ΔP, pressure drop; Stokes number at the 50% cut-off diameter is calculated as: $Stk_{50} = \frac{4\rho_p Q d_p^2 Cc}{9\pi n \mu W^3}$, where d_p is the particle diameter, and *Cc* is Cunningham slip correction factor.

Table 4-2: Effects of loading on collection efficiency of the impaction stage.

Particle Diameter [nm]	**Prior Impactor Loading [mg/m^3×hr]**		
	0	13.6	21.5
	Collection Efficiency (StDev)		
15	0.26 (0.08)	0.11 (0.08)	0.15 (0.06)
50	0.12 (0.02)	0.08 (0.04)	0.07 (0.02)
80	0.07 (0.01)	0.07 (0.04)	0.04 (0.01)
100	0.08 (0.03)	0.09 (0.02)	0.06 (0.02)
300	0.54 (0.02)	0.57 (0.01)	0.57 (0.08)
500	0.90 (0.03)	0.89 (0.01)	0.86 (0.07)
800	0.98 (0.02)	0.97 (0.01)	0.92 (0.08)
1000	0.99 (0.01)	0.97 (0.01)	0.93 (0.07)

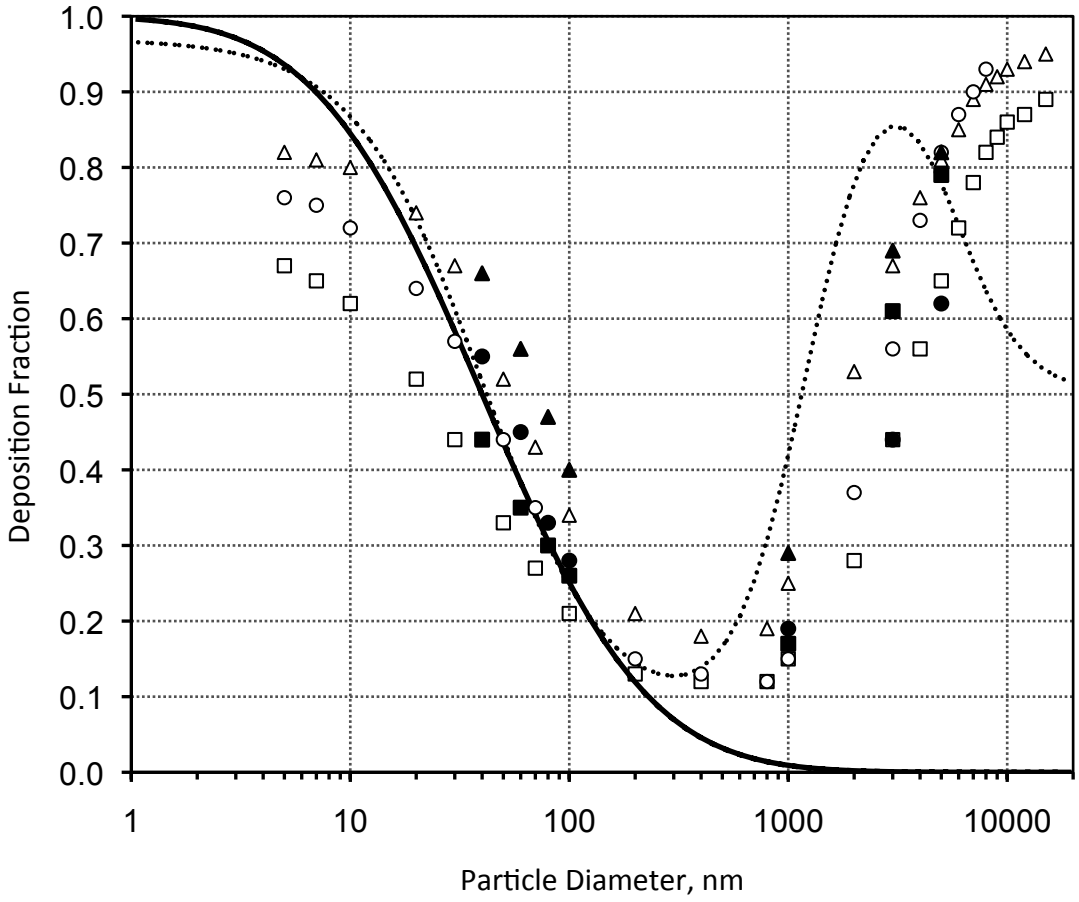

Figure 4-1: Total deposition fraction vs. particle diameter.

Note: ― is the NPM criterion; ···· is deposition in all regions of the respiratory tract as defined by the ICRP. All other symbols are deposition fraction in the normal lung at FRC=3000 ml for controlled breathing patterns. Open symbols are data from Heyder et al. (1986): □ is Vt=500 ml, Q=250 ml/s; Δ is Vt=1000 ml, Q=250 ml/s; ○ is Vt=1000 ml, Q=500 ml/s. Closed symbols are data of Kim and Hu (1998) and Kim and Jaques (2000): ■ is Vt=500 ml, Q=250 ml/s; ▲ is Vt=1000 ml, Q=250 ml/s; ● is Vt=1000 ml, Q=500 ml/s. Vt=tidal breathing volume and Q=air flow rate.

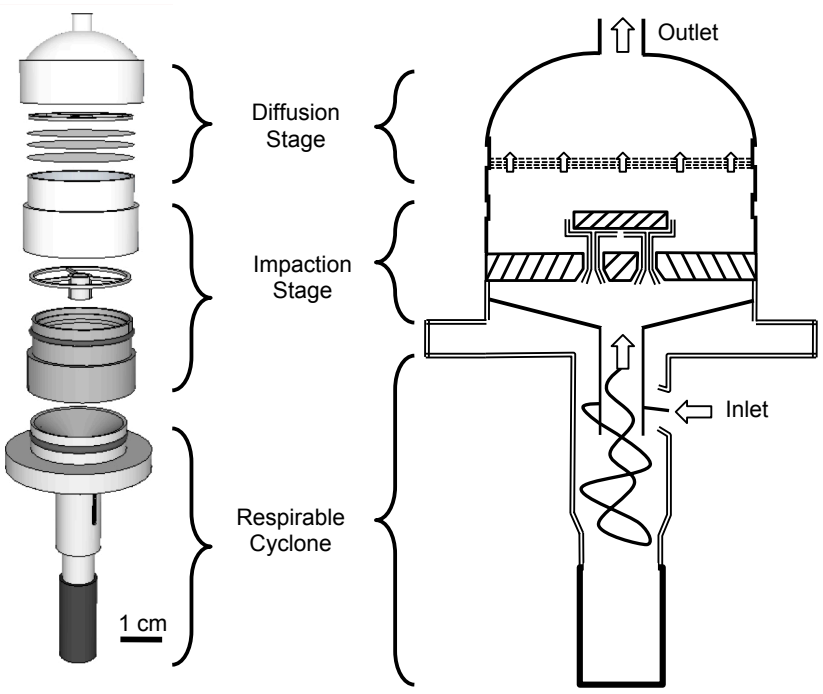

Figure 4-2: The components and schematic drawing with airflow paths of the NRD sampler.

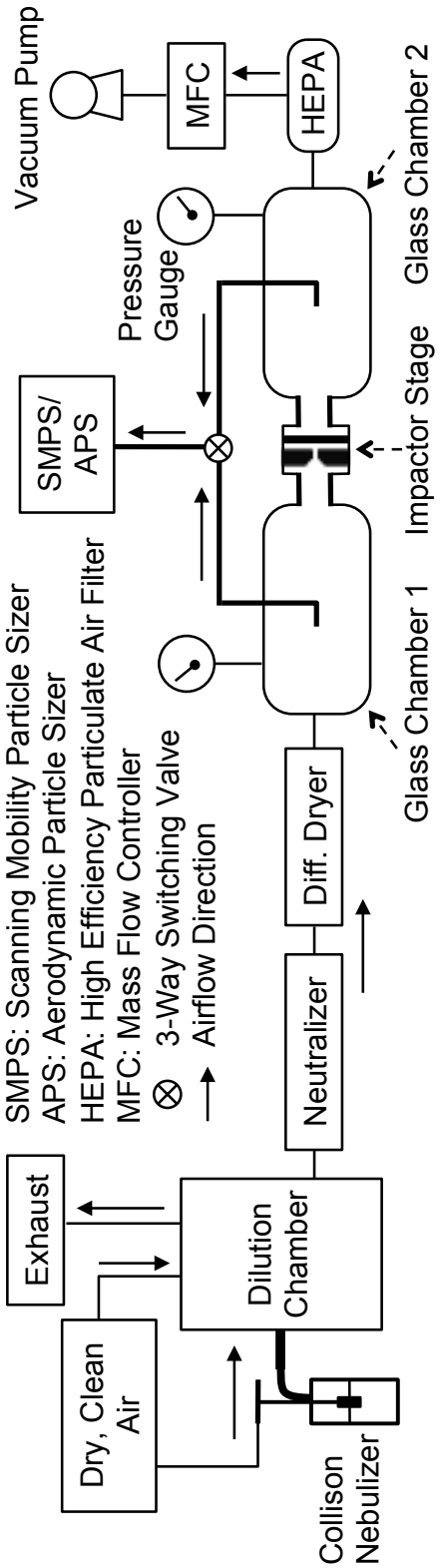

Figure 4-3: Experimental setup for the impaction stage evaluation.

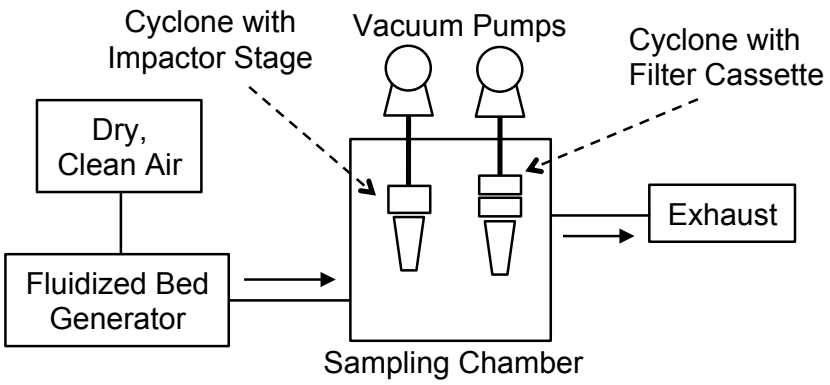

Figure 4-4: Experimental setup for the impactor loading tests.

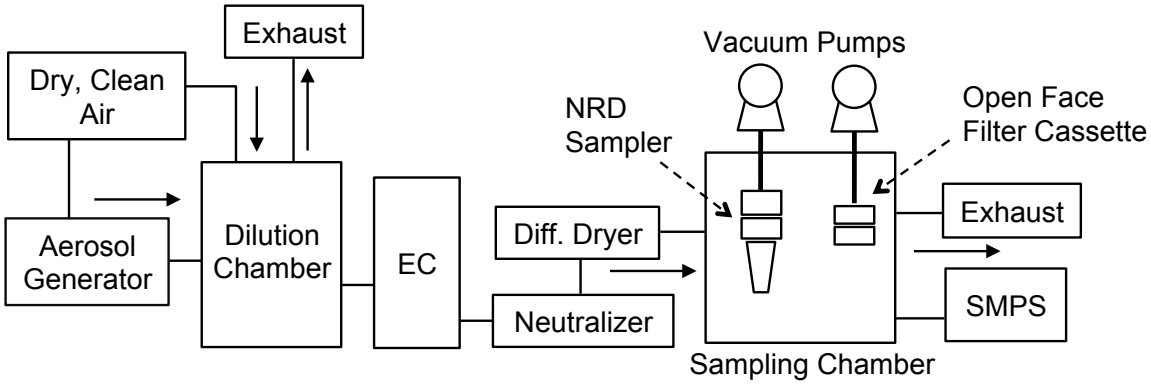

Figure 4-5: Experimental setup for the diffusion stage deposition tests.

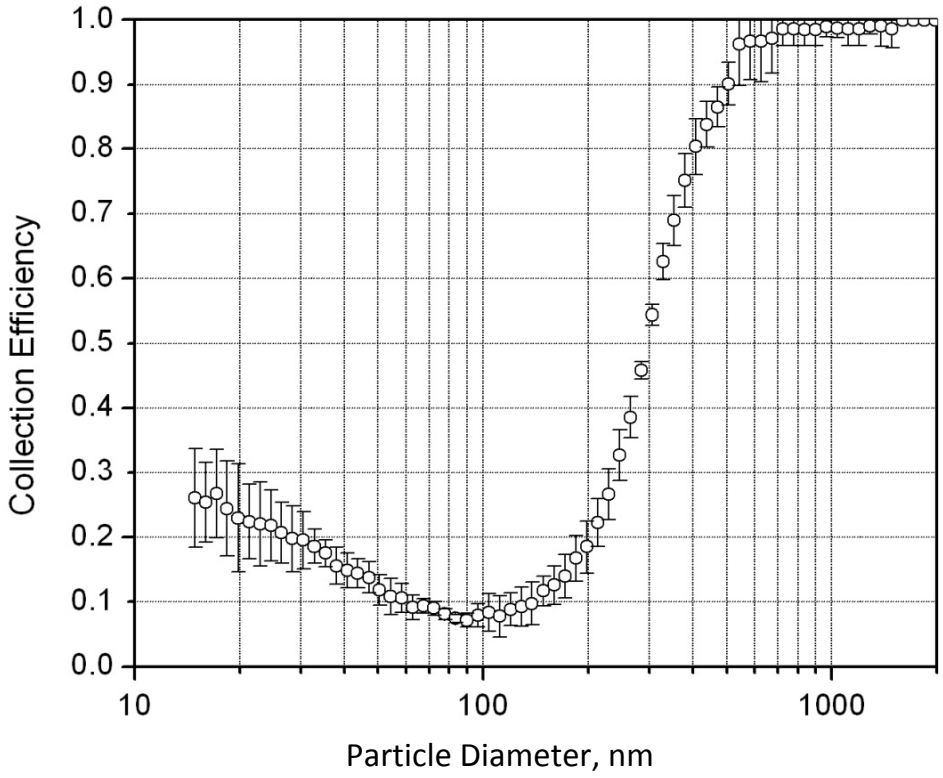

Figure 4-6: Collection efficiency by size of the impaction stage.

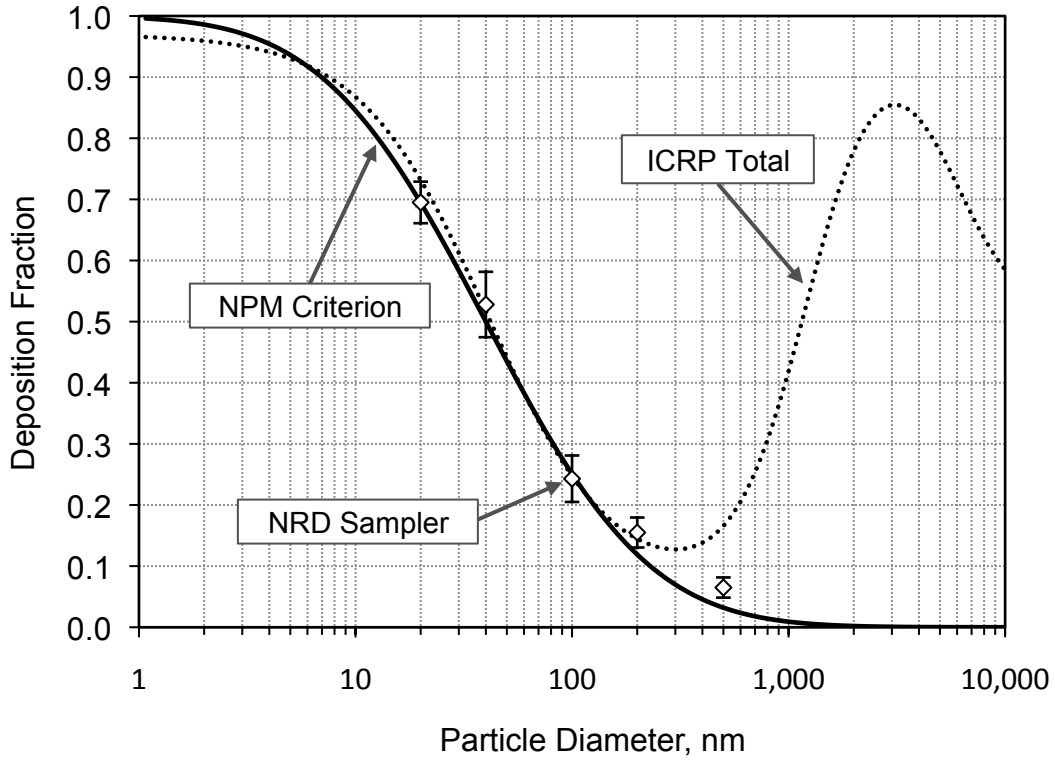

Figure 4-7: NPM sampling criterion, ICRP total respiratory deposition and effective deposition on the diffusion stage of the NRD sampler.

CHAPTER V

CONCLUSIONS

The work presented in this doctoral dissertation accomplishes two goals: 1) it provides knowledge on workers' exposure to nanoparticles that was gained by conducting a field study (Chapter II); and 2) it assists in the development of standard methods to assess the presence of nanoparticles in workplace environments through two laboratory studies (Chapters III and IV).

The field study was conducted in a facility that manufactures CNT-composite nanomaterials. A review of the literature revealed very little knowledge of workers' exposure to particulate matter occurring during manufacturing and mechanical processing of CNT-composite nanomaterials. Additionally, characterization of particles generated during mechanical processing of these composite nanomaterials is not available in the literature. The findings of the first study, presented in Chapter II of this dissertation, show that transferring by scooping bulk CNTs between containers during a simulated weighing process does not generate appreciable aerosol concentrations above background measurements. Manual sanding of epoxy containing CNTs generates micron-sized particles with CNTs protruding from the particle core, not nanoparticles. No CNTs were observed free from composite material, indicating consistency with observations made by others on asbestos fibers. Thus, CNT fibers encapsulated or bonded with other materials may have limited potential for airborne release. This study also showed that enclosures have a significant effect on particle release and that biological safety cabinets are an effective enclosure for minimizing workers' exposure during CNT-composite sanding. Performing the sanding task inside a custom fume hood was found to release more particles in the operator's breathing zone than when no ventilation controls were in place. The poor performance of the custom fume hood observed in this study may have been caused by the formation of turbulent currents in front of the operator, which have been

found to pull contaminants out of the hood and in the worker's breathing zone, and may also have been exacerbated by the poor hood design. Thus, proper enclosure design and selection play an important role in workers' exposure to CNT-composite particulate matter during manual sanding. From this fieldwork we recognized that direct-read instruments have several limitations that could be overcome with the development of a personal sampler for nanoparticles. These limitations include particle losses in the sampling probes placed in the operator's breathing zone to carry the aerosol to the instruments and the limited portability of the instruments to follow worker's movements.

Chapter IV of this dissertation described the development of a sampling criterion for nano-particualte matter (NPM) and the subsequent development and laboratory testing of a nanoparticle respiratory deposition (NRD) sampler. Current filter-based samplers are inadequate for collecting nanoparticles separately from larger particles, and personal dose-samplers that selectively collect nanoparticles and mimic nanoparticle deposition in the respiratory system are unavailable. The absence of a collection criterion for nanoparticles is a limiting factor in selecting a standard to which a nanoparticle sampler should conform. Experimental data on lung deposition has provided useful insights on nanoparticle deposition in the respiratory system, found to be in agreement with the ICRP total lung deposition model. The ICRP model was thus selected as the foundation for the development of the NPM sampling criterion. The curve was fit to match total deposition of particles smaller than 300 nm selecting the same mathematical form as that used for the thoracic and respirable sampling criteria. This new criterion, however, ties sampler performance to the total deposition of nanoparticles in the respiratory tract and was set as the target for the development of the NRD sampler.

The NRD sampler consists of a respirable cyclone fitted with a custom impactor with a d_{50} = 300 nm and a diffusion stage containing eight nylon mesh screens. The sampler fits on a worker's lapel and is designed to sample for the duration of an entire work-shift. Theoretical collection efficiency of the nylon mesh screens used in the

diffusion stage was tested and modified in the study reported in Chapter III. Additionally, in this study the morphology of silver particles smaller than 100 nm was found to have minimal effect on the collection efficiency of nylon mesh screens. The deposition efficiency of the diffusion stage of the NRD sampler mimics deposition of nanoparticles in the respiratory tract by following the NPM criterion. The NRD sampler can be easily modified to match future revisions of this collection criterion. This personal sampler can provide valuable information on personal exposure to nanoparticles and contribute to the development of toxicological and epidemiological studies and of standards for exposure to nanoparticles.

Future work

The work presented in Chapter II on exposure to CNT-composite particles was a field study in an industrial facility with limited ability to control experimental variables and, therefore, had some design limitations that can be addressed in future studies. Controlled laboratory simulations of the mechanical processing of CNT-composite nanomaterials can provide adequate repetition of the processes. These repetitions would provide statistical parameters representative of what is expected when a task is repeated several times. The controlled simulations should also determine how process details (e.g., amount of pressure placed on the samples, sanding speed) affect the generation of particulate matter. Furthermore, they should establish how the amount of material dispersed from the sandpaper or other tools used during the mechanical process contribute to aerosol measurements. Exposure should also be measured and characterized during other mechanical processes such as drilling or cutting of the CNT-composite nanomaterial. Additionally, these exposure measurements in the field and in laboratory simulations should be extended to the various steps of the manufacturing of products that contain engineered nanoparticles other than CNTs. Future exposure measurements in a controlled laboratory setting should also consider measurements of the frequency of air

exchanges in the room and attempt to characterize and control airflow patterns in the room and around the workers.

Extension of the laboratory tests performed on the nylon mesh screens (Chapter III), and on the NRD sampler (Chapter IV), should involve the development of techniques for the recovery and analysis of the particles collected onto the nylon screens used in the diffusion stage. Laboratory tests should be conducted to optimize an analysis method to detect nanoparticles. These tests may begin with assessing detection of TiO_2 nanoparticles by inductively couple plasma mass spectrometry. The limits of detection and quantification of the method should be established and the method should then be expanded and tested for precision for analysis of other nanoparticles of commercial interest (e.g., Ag, CuO, ZnO). Alternative collection media for the diffusion stage may also be tested in an attempt to lower the number of layers of media necessary to achieve the target collection efficiency. Excessive amount of collection substrate media interferes with the analysis and lowers the limit of detection.

The NRD sampler is to be employed next in field studies. The sampler should be deployed in large quantities and used to evaluate the extent to which workers are exposed to nanoparticles. The NRD sampler with its sampling and analysis methods should be used in epidemiological studies that investigate the relationship of nanoparticle exposures to adverse health effects in both occupational and environmental settings.

APPENDIX A:

PILOT DESIGNS OF THE IMPACTION STAGE

The initial design of the impaction stage consisted of three circular jets with width W=0.45 mm and circular polyurethane foam (PUF) impaction substrate. This substrate was originally selected because it had been found to minimize particle bounce avoiding the use of adhesives (Kavouras and Koutrakis, 2001; Demokritou et al., 2002, 2004a and b; Lee et al., 2005). The d_{50} of this first design of the impactor stage corresponded to the impactor's design specifications and was experimentally measured at 300 nm. Our tests (Figure A-1), however, indicated poor collection efficiency of the PUF substrate above the d_{50} cut-off.

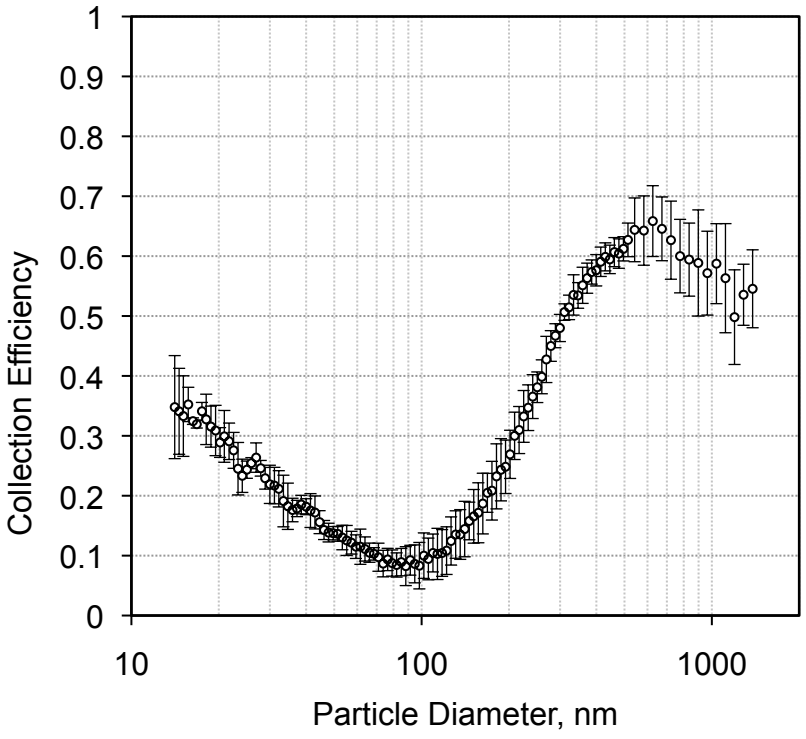

Figure A-1: Collection efficiency by size of the first impaction stage prototype.

A second design of the impaction stage consisted of equivalent jet width (W=0.45 mm) but an impaction plate made of solid aluminum. This design resulted in better performance (Figure A-2) but smaller cut-off (d_{50} = 220 nm) than desired, and led to the modification of the jet width in the third and final design described in Chapter IV. The pressure drop of these first prototypes of the impactor stage was substantially higher (5 kPa, 20 in. H_2O) than the final design (2.49 kPa, 10 in. H_2O).

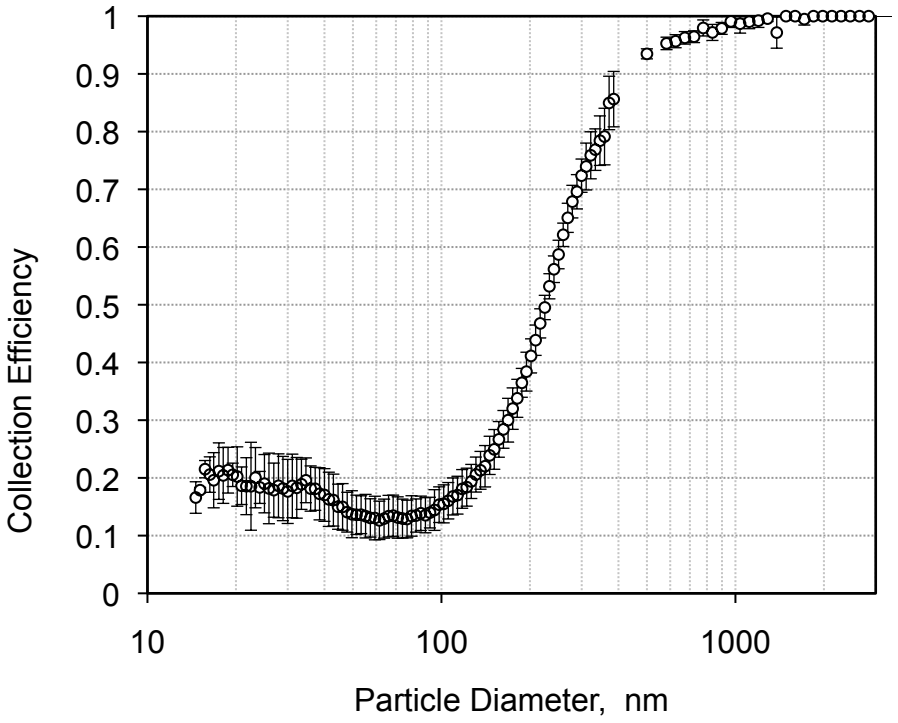

Figure A-2: Collection efficiency by size of the second impaction stage prototype.

REFERENCES

American Conference of Governmental Industrial Hygienists (ACGIH). (2007). *2007 Industrial ventilation-A manual of recommended practices* (26th ed.). Cincinnati, OH: ACGIH.

American Conference of Governmental Industrial Hygienists (ACGIH). (2010). *TLVs and BEIs based on the documentation of the threshold limit values for chemical substances and physical agents and biological exposure indices*. Cincinnati, OH: ACGIH.

American National Standards Institute (ANSI)/American Society of Heating Refrigeration and Air Conditioning Engineers (ASHRAE). (1995). *Method of testing performance of laboratory fume hoods* [Standard]. ANSI/ASHRAE Standard 110–1995. Atlanta, GA: ANSI/ASHRAE.

American Society for Testing and Materials (ASTM). (2006). Standard terminology relating to nanotechnology. ASTM Standard E2456. West Conshohocken, PA: ASTM International.

Baron, P. A., & Willeke, K. (2001a). *Aerosol measurement: Principles, techniques, and applications* (2nd ed.), New York, NY: John Wiley and Sons, Inc.

Baron, P. A., & Willeke, K. (2001b). Gas and particle motion. In P. A. Baron & K. Willeke (Eds.), *Aerosol measurement: Principles, techniques, and applications* (2nd ed., pp. 61-82). New York, NY: John Wiley and Sons, Inc.

Baron, P. A., Maynard, A. D., & Foley, M. (2003). Evaluation of aerosol release during the handling of unrefined single walled carbon nanotube material. National Institute for Occupational Safety and Health (NIOSH) Report. NIOSH DART-02-191/ NTIS PB2003–102401. Cincinnati, OH: NIOSH.

Bastian, S., Busch, W., Kühnel, D., Springer, A., Meibner, T., Holke, R.,… Schirmer, K. (2009). Toxicity of tungsten carbide and cobalt-doped tungsten carbide nanoparticles in mammalian cells in vitro. *Environmental Health Perspectives.* 117(4), 530-436.

Bello, D., Hart, J. A., Ahn, K., Hallock, M., Yamamoto, N., Garcia, E. J., . . . Wardle, B. L. (2008). Particle exposure levels during CVD growth and subsequent handling of vertically-aligned carbon nanotube films. *Carbon*, 46, 974-981.

Bello, D., Wardle, B. L., Yamamoto, N., deVillora, R. G., Garcia, E. J., Hart, A. J., . . . Hallock, M. (2009). Exposure to nanoscale particles and fibers during machining of hybrid advanced composites containing carbon nanotubes. *Journal of Nanoparticle Research*, 11, 231- 249.

Brockmann, J. E. (2001). Sampling and transport of aerosol. In P. A. Baron & K. Willeke (Eds.), *Aerosol measurement: Principles, techniques, and applications* (2nd ed., pp. 143-195). New York, NY: John Wiley and Sons, Inc.

Cha, K., Hong, H. W., Choi, Y. G., Lee, M. J., Park, J. H., Chae, H. K., . . . Myung, H. (2008). Comparison of acute responses of mice livers to short-term exposure to nano-sized or micro-sized silver particles. *Biotechnology Letters*, 30(11), 1893-1899.

Chen, S. C., & Tsai, C. J. (2007). An axial flow cyclone to remove nanoparticles at low pressure conditions. *Journal of Nanoparticle Research,* 9(1), 71-83.

Chen, Z., Meng, H. A., Xing, G. M., Chen, C. Y., Zhao, Y. L., Jia, G. A., . . . Wan, L. J. (2006). Acute toxicological effects of copper nanoparticles in vivo. *Toxicology Letters*, 163(2), 109-120.

Cheng, Y. S. (2001). Condensation detection and diffusion size separation techniques. In P. A. Baron & K. Willeke (Eds.), *Aerosol measurement: Principles, techniques, and applications* (2nd ed., pp. 569-601). New York, NY: John Wiley and Sons, Inc.

Cheng, Y. S., & Yeh, H. C. (1980). Theory of a screen-type diffusion battery. *Journal of Aerosol Science*, 11, 313-320.

Cheng, Y. S., and Yeh, H. C. (1983). Performance of a screen-type diffusion battery. In V. A. Marple & B. Y. H. Liu (Eds.), *Aerosols in mining and industrial work environments: Instrumentation* (pp. 1077-1094). Ann Arbor, MI: Ann Arbor Science.

Cheng, Y. S., Keating, J. A., & Kanapilly, G. M. (1980). Theory and calibration of a screen-type diffusion battery. *Journal of Aerosol Science*, 11, 549-556.

Cheng, Y. S., Yeh, H. C., & Brinsko, K. J. (1985). Use of wire screens as a fan model filter. *Aerosol Science and Technology*, 4, 165–174.

Choi, J. I., & Kim, C. S. (2007). Mathematical analysis of particle deposition in human lungs: An improved single path transport model. *Inhalational Toxicology*, 19, 925-939.

Daigle, C. C., Chalupa, D. C., Gibb, F. R., Morrow, P. E., Oberdorster, G., Utell, M. J., & Frampton, M. W. (2003). Ultrafine particle deposition in humans during rest and exercise. *Inhalation Toxicology*, 15, 539–552.

Demokritou, P., Gupta, T., Ferguson, S. T., & Koutrakis, P. (2002). Development and laboratory performance evaluation of a personal cascade impactor. *Journal of the Air & Waste Management Association*, 52, 1230–1237.

Demokritou, P., Lee, S. J., & Koutrakis, P., (2004a). Development and evaluation of a high loading PM2.5 speciation sampler. *Aerosol Science and Technology*, 38, 111–119.

Demokritou, P., Lee, S. J., Ferguson, S. T., & Koutrakis, P. (2004b). A compact multistage (cascade) impactor for the characterization of atmospheric aerosols. *Journal of Aerosol Science*, 35, 281–299.

Donaldson, K., Stone, V., Gilmour, P. S., Brown, D. M., & MacNee, W. (2000). Ultrafine particles: Mechanisms of lung injury. *The Royal Society*, 358, 2741-2749.

Duffin, R., Tran, L., Brown, D., Stone, V., & Donaldson, K. (2007). Proinflammogenic effects of low-toxicity and metal nanoparticles in vivo and in vitro: Highlighting the role of particle surface area and surface reactivity. *Inhalation Toxicology*, 19(10), 849-856.

Elihn, K., & Berg, P. (2009). Ultrafine particle characteristics in seven industrial plants. *The Annals of Occupational Hygiene*, 53(5), 475-484.

Emi, H., Wang, C. S., & Tien, C. (1982). Transient behavior of aerosol filtration in model filters. *AIChE Journal*, 28, 397-405.

Esmen, N. A., Johnson, D. L., & Agron, G. M. (2002). The variability of delivered dose of aerosols with the same respirable concentration but different size distributions. *The Annals of Occupational Hygiene*, 46, 401–7.

European Committee for Standardization (CEN). (1993). *Workplace atmospheres: Size fraction definitions for measurement of airborne particles*. CEN Standard EN 481. Brussels: CEN

Evans, D. E., Ku, B. K., Birch, M. E., & Dunn, K. H. (2010). Aerosol monitoring during carbon nanofiber production: Mobile direct-reading sampling. *The Annals of Occupational Hygiene*, 54(5), 514-531.

Ferin, J., Oberdörster, G., & Penney, D. P. (1992). Pulmonary retention of ultrafine and fine particles in rats. *American Journal of Respiratory Cell and Molecular Biology*, 6, 535–542.

Friedlander, S. K. (1958). Theory of aerosol filtration. *Industrial & Engineering Chemistry*, 50(8), 1161-1164.

Fu, T. H., Cheng, M. T., & Shaw D. T. (1990). Filtration of chain aggregate aerosols by model screen filter. *Aerosol Science and Technology*, 13, 151-161.

Furuuchi, M., Eryu, K., Nagura, M., Mitsuhiko, H., Kato, T., Tajima, N., . . . Otani, Y. (2010). Development and performance evaluation of air sampler with inertial filter for nanoparticle sampling. *Aerosol and Air Quality Research*, 10, 185–192.

Gentry, J. W., & Choudhary, K. R. (1975). Collection efficiency and pressure drop in grid filters of high packing densities at intermediate Reynolds numbers. *Journal of Aerosol Science*, 6, 277-290.

Gorbunov, B., Priest, N. D., Muir, R. B., Jackson, P. R., & Gnewuch, H. (2009). A novel size-selective airborne particle size fractionating instrument for health risk evaluation. *The Annals of Occupational Hygiene*, 53(3), 225-237.

Grassian, V. H. (2008). When size really matters: Size-dependent properties and surface chemistry of metal and metal oxide nanoparticles in gas and liquid phase environments. *Journal of Physical Chemistry C*, 112(47), 18303-18313.

Grassian, V. H., Adamcakova-Dodd, A., Pettibone, J. M., O'Shaughnessy, P. T. and Thorne, P. S. (2007). Inflammatory response of mice to manufactured titanium dioxide nanoparticles: Comparison of size effects through different exposure routes. *Nanotoxicology*, 1(3), 211-226.

Grohse, P. M. (1999). Trace element analysis of airborne particles by atomic absorption spectroscopy, inductively coupled plasma-atomic emission spectroscopy, and inductively coupled plasma-mass spectrometry. In S. Landsberger & M. Creatchman (Eds.), *Environmental analysis of airborne particles. Advances in environmental, industrial and process control technologies* (Vol. 1, pp. 1-65), The Netherlands, Amsterdam: Gordon and Breach Science Publishers.

Han, J. H., Lee, E. J., Lee, J. H., So, K. P., Lee, Y. H., Bae, G. N., . . . Yu, I. J. (2008). Monitoring multiwalled carbon nanotube exposure in carbon nanotube research facility. *Inhalation Toxicology*, 20(8), 741-749.

Hansen, S. F., Michelson, E. S., Kamper, A., Borling, P., Stuer-Lauridsen, F., & Baun, A. (2008). Categorization framework to aid exposure assessment of nanomaterials in consumer products. *Ecotoxicology*, 17, 438-447.

Hering, S. V., & Marple, V. (1986). Low pressure and micro-orifice impactors (Ch. 5). In J. P. Lodge & T. L. Chan (Eds.), *Cascade impactors*. Akron, Ohio: American Industrial Hygiene Association (AIHA).

Hering, S. V., Flagan, R. C., & Friedlander, S. K. (1978). Design and evaluation of new low-pressure impactor, 1. *Environmental Science & Technology*, 12(6), 667-673.

Hering, S. V., Friedlander, S. K., Collins, J. J, & Richards, L. W. (1979). Design and evaluation of a new low-pressure impactor, 2. *Environmental Science & Technology*, 13(2), 184-188.

Heyder, J., Gebhart, J., Rudolf, G., Schiller, C. F., & Stahlhofen, W. (1986). Deposition of particles in the human respiratory tract in the size range 0.005–15 μm. *Journal of Aerosol Science*, 17, 811–825.

Hillamo, R. E, & Kauppinen, E. I. (1991). On the performance of the Berner low pressure impactor. *Aerosol Science and Technology*, 14, 33-47.

Hinds, W. C. (1999). *Aerosol technology: Properties, behavior, and measurement of airborne particles.* New York, NY: John Wiley & Sons, Inc.

Hodgkins D. G., Robins, T. G., Hinkamp, D. L., Schork, M. A., Levine, S. P., & Krebs, W. H. (1991). The effect of airborne lead particle size on worker blood-lead levels: An empirical study of battery workers. *Journal of Occupational and Environmental Medicine*, 33, 1265–1273.

Huang, R. F., & Chou, C. I. (2009). Flow and performance of an air-curtain biological safety cabinet. *The Annals of Occupational Hygiene*, 53(4), 425-440.

Hubbs, A. F., Mercer, R. R., Coad, J. E., Battelli, L. A., Willard, P., Sriram, K., . . . Porter, D. (2009). Persistent pulmonary inflammation, airway mucous metaplasia and migration of multi-walled carbon nanotubes from the lung after subchronic exposure. *The Toxicologist*, 108, A2193.

Iijima, S. (1991). Helical microtubules of graphitic carbon. *Nature*, 354(7), 56-58.

International Commission on Radiological Protection (ICRP). (1994). *Human respiratory tract model for radiological protection* (Publication 66). Oxford, UK: Elsevier Science, Ltd.

International Organization for Standardization (ISO). (1995). *Air quality: Particle size fraction definitions for health-related sampling* (ISO Standard 7708). Geneva: International Organization for Standardization.

International Organization for Standardization (ISO). (2008). *Nanotechnologies: Terminology and definitions for nano-object: Nanoparticle, nanofibre and nanoplate* (ISO/TS 27687). Geneva: International Organization for Standardization.

Jaques, P. A., & Kim, C. S. (2000). Measurement of total lung deposition of inhaled ultrafine particles in healthy men and women. *Inhalation Toxicology*, 12, 715–731.

Jiang, J. K., Oberdörster, G., & Biswas, P. (2009). Characterization of size, surface charge, and agglomeration state of nanoparticle dispersions for toxicological studies. *Journal of Nanoparticle Research*, 11(1), 77-89.

Jiang, J., Oberdörster, G., Elder, A., Gelein, R., Mercer, P., & Biswas, P. (2008). Does nanoparticle activity depend upon size and crystal phase? *Nanotoxicology*, 2(1), 33-42.

Johnson, D. L., & Esmen, N. A. (2004) Method-induced misclassification for a respirable dust sampled using ISO/ACGIH/CEN criteria. *The Annals of Occupational Hygiene*, 48, 13–20.

Johnson, D. R., Methner, M. M., Kennedy, A. J., & Stevens, J. A. (2010). Potential for occupational exposure to engineered carbon-based nanomaterials in environmental laboratory studies. *Environmental Health Perspectives*, 118(1), 49-54.

Karlsson, H. L., Gustafsson, J., Cronholm, P., & Moller, L. (2009). Size-dependent toxicity of metal oxide particles: A comparison between nano- and micrometer size. *Toxicology Letters*, 188(2), 112-118.

Kavouras, I. G., & Koutrakis, P. (2001). Use of polyurethane foam as the impaction substrate/collection medium in conventional inertial impactors. *Aerosol Science and Technology*, *34*, 46–56.

Kim, C. S., and Hu, S. C. (1998). Regional deposition of inhaled particles in human lungs: Comparison between men and women. *Journal of Applied Physiology.* 84, 1834–1844.

Kim, C. S., and Jaques, P. A. (2000). Respiratory dose of inhaled ultrafine particles in healthy adults. *Philosophical Transactions of the Royal Society of London,* A 358, 2693– 2705.

Kim, S. C., Wang, J., Emery, M. S., Shin, W. G., Mulholland, G. W., & Pui, D. Y. H. (2009). Structural property effect of nanoparticle agglomerates on particle penetration through fibrous filter. *Aerosol Science and Technology*, 43, 344–355.

Kim, T., & Flynn, M. R. (1991) Airflow pattern around a worker in a uniform freestream. *American Industrial Hygiene Association Journal*, 52(7), 287-296.

Kirsch, A. A., & Fuchs, N. A. (1967). Studies on fibrous aerosol filters-II. Pressure drops in systems of parallel cylinders. *The Annals of Occupational Hygiene*, 10, 23-30.

Kirsch, A. A., & Fuchs, N. A. (1968). Studies on fibrous filters-III. Diffusional deposition of aerosols in fibrous filters. *The Annals of Occupational Hygiene*, 11, 299-304.

Kirsch, A. A., & Stechkina, I. B. (1978). The theory of aerosol filtration with fibrous filters. In D. T. Shaw (Ed.), *Fundamentals of aerosol science* (pp. 165-256). New York, NY: John Wiley & Sons, Inc.

Kisin, E., Murray, A. R., Schwegler-Berry, D., Scabilloni, J., Mercer, R. R., Chirila, M., . . . Shvedova, A. A. (2010). Pulmonary response, oxidative stress and genotoxicity induced by carbon nanotubes. *The Toxicologist*, 114, A793.

Kleinstreuer, C., Zhang, Z., & Donohue, J. F. (2008). Targeted drug-aerosol delivery in the human respiratory system. *Annual Review of Biomedical Engineering*, 10, 195-220.

Koehler, K. A., Clark, P., & Volckens, J. (2009). Development of a sampler for total aerosol deposition in the human respiratory tract. *The Annals of Occupational Hygiene*, 53(7), 731–738.

Köhler, A. R., Som, C., Helland, A., & Gottschalk, F. (2008). Studying the potential release of carbon nanotubes throughout the application life cycle. *Journal of Cleaner Production*, 16, 927-937.

Kruse, R. H., Puckett, W. H., & Richardson, J. H. (1991). Biological safety cabinetry. *Clinical Microbiology Reviews*, 4(2), 207-241.

Ku, B. K., & Maynard, A. D. (2006). Generation and investigation of airborne silver nanoparticles with specific size and morphology by homogeneous nucleation, coagulation and sintering. *Journal of Aerosol Science*, 37, 452–470.

Kuhlbusch, T. A., Neumann, S., & Fissan, H. (2004). Number size distribution, mass concentration, and particle composition of PM1, PM2.5, and PM10 in bag filling areas of carbon black production. *Journal of Occupational and Environmental Hygiene*, 1(10), 660–671.

Kuo, Y. M. Huang, S. H. Shih, T. S., Chen, C. C., Weng, Y. M., Lin, W. Y. (2005). Development of a size-selective inlet-simulating ICRP lung deposition fraction. *Aerosol Science and Technology*, 39, 437–443. doi: 10.1080/027868290956602

Lam, C. W., James, J. T., McCluskey, R., & Hunter, R. L. (2004). Pulmonary toxicity of single-wall carbon nanotubes in mice 7 and 90 days after intratracheal instillation. *Toxicological Sciences*, 77, 126–134.

Lam, C., James, J. T., McCluskey, R., Arepalli, S., & Hunter, R. L. (2006). A review of carbon nanotube toxicity and assessment of potential occupational and environmental health risks. *Critical Reviews in Toxicology*, 36(3), 189-217.

Lau, A. K., & Hui, D. (2002). The revolutionary creation of new advanced materials—Carbon nanotube composites. *Composites Part B: Engineering*, 33(4), 263-277.

Lee, J. H., Lee, S. B., Bae, G. N., Jeon, K. S., Yoon, J. U., Ji, J. H., . . . Yu, I. J. (2010). Exposure assessment of carbon nanotube manufacturing workplaces. *Inhalation Toxicology*, 22(5), 369-381.

Lee, S. J., Demokritou, P., & Koutrakis, P. (2005). Performance evaluation of commonly used impaction substrates under various loading conditions. *Journal of Aerosol Science*, 36(7), 881-895.

Li, Z., Huldermen, T., Salmen, R., Chapman, R., Leonard, S. S., Young, S. H., . . . Simeonova, P. P. (2007). Cardiovascular effects of pulmonary exposure to single-wall carbon nanotubes. *Environmental Health Perspectives*, 115(3), 377-382.

Liu, P. S. K., & Deshler, T. (2003). Causes of concentration differences between a scanning mobility particle sizer and a condensation particle counter. *Aerosol Science and Technology*, 37, 916–923.

Löndahl, J., Massling, A., Pagels, J., Swietlicki, E., Vaclacik, E., & Loft, S. (2007). Size-resolved respiratory-tract deposition of fine and ultrafine hydrophobic and hygroscopic aerosol particles during rest and exercise. *Inhalation Toxicology*, 19, 109–116.

Löndahl, J., Massling, A., Swietlicki, E., Brauner, E. V., Ketzel, M., Pagels, J., & Loft, S. (2009). Experimentally determined human respiratory tract deposition of airborne particles at a busy street. *Environmental Science & Technology*, 43(13), 4659-4664.

Löndahl, J., Pagels, J., Boman, C., Swietlicki, E., Massling, A., Rissler, J., . . . Sandström, T. (2008). Deposition of biomass combustion aerosol particles in the human respiratory tract. *Inhalation Toxicology*, 20(10), 923-933. doi:10.1080/08958370802087124.

Lwebuga-Mukasa, J. S., Oyana, T. J., & Johnson, C. (2005). Local ecological factors, ultrafine particulate concentrations, and asthma prevalence rates in Buffalo, New York, neighborhoods. *Journal of Asthma*, 42(5), 337-48.

Magari, S. R., Hauser, R., Schwartz, J., Williams, P. L., Smith, T. J., & Christiani, D. C. (2001). Association of heart rate variability with occupational and environmental exposure to particulate air pollution. *Circulation*, 104, 986-991.

Marple V. A., Olson, B. A., & Rubow, K. L. (2001). Inertial, gravitational, centrifugal, and thermal collection techniques. In P. A. Baron & K. Willeke (Eds.), *Aerosol measurement: Principles, techniques, and applications* (2nd ed., pp. 229-260). New York, NY: John Wiley and Sons, Inc.

Marple, V. A., & Willeke, K. (1976). Impactor design. *Atmospheric Environment*, 12, 891-896.

Marple, V. A., Rubow, K. L., & Behm, S. M. (1991). A microorifice uniform deposit impactor (MOUDI): Description, calibration, and use. *Aerosol Science and Technology*, 14(4), 434-446.

Maynard, A. D. (2007). Nanotechnology: The next big thing, or much ado about nothing? *The Annals of Occupational Hygiene*, 51(1), 1-12.

Maynard, A. D., & Jensen, P. A. (2001). Aerosol measurement in the workplace. In P. A. Baron & K. Willeke (Eds.), *Aerosol measurement: Principles, techniques, and applications* (2nd ed., pp. 779-799). New York, NY: John Wiley and Sons, Inc.

Maynard, A. D., Baron, P. A., Foley, M., Shvedova, A. A., Kisin, E. R., & Castranova, V. (2004). Exposure to carbon nanotube material: Aerosol release during the handling of unrefined single walled carbon nanotube material. *Journal of Toxicology and Environmental Health*, 67(1), 87-107.

Mercer, R. R., Hubbs, A. F., Scabilloni, J. F., Wang, L., Battelli, L. A., Schwegler-Berry D., . . . Porter, D. W. (2010). Distribution and persistence of pleural penetrations by multi-walled carbon nanotubes. *Particle and Fibre Toxicology*, 7(28), 1-11.

Methner, M. M., Birch, M. E., Evans, D. E., Ku, B. K., Crouch, K. G., & Hoover, M. D. (2007). L. F. Mazzuckelli (Ed.), Case study: Identification and characterization of potential sources of worker exposure to carbon nanofibers during polymer composite laboratory operations. *Journal of Occupational and Environmental Hygiene*, 4(12), D125-D130.

Methner, M., Hodson, L., Dames, A., & Geraci, C. (2010a). Nanoparticle emission assessment technique (NEAT) for the identification and measurement of potential inhalation exposure to engineered nanomaterials—part B: Results from 12 field studies. *Journal of Occupational and Environmental Hygiene*, 7(3), 163–176. doi: 10.1080/15459620903508066

Methner, M., Hodson, L., & Geraci, C. (2010b). Nanoparticle emission assessment technique (NEAT) for the identification and measurement of potential inhalation exposure to engineered nanomaterials—part A. *Journal of Occupational and Environmental Hygiene*, 7(3), 127–132. doi: 10.1080/15459620903476355

Misra, C., Singh, M., Shen, S., Sioutas, C., Hall, P. M. (2002). Development and evaluation of a personal cascade impactor sampler (PCIS). *Aerosol Science*, 33, 1027–1047.

Monteiro-Riviere, N. A., Nemanich, R. J., Inman, A. O., Wang, Y. Y., & Riviere, J. E. (2005). Multi-walled carbon nanotube interactions with human epidermal keratinocytes. *Toxicology Letters*, 155, 377-384.

Montoya, L. D., Lawrence, J., Murthy, G. G. K., Sarnat, J. A., Godleski, J. J., & Koutrakis, P. (2004). Continuous measurements of ambient particle deposition in human subjects. *Aerosol Science and Technology*, 38(10), 980-990.

Mowat, F., Bono, M., Lee, R. J., Tamburello, S., & Paustenbach, D. (2005). Occupational exposure to airborne asbestos from phenolic molding material (bakelite) during sanding, drilling, and related activities. *Journal of Occupational and Environmental Hygiene*, 2, 497–507.

Muller, J., Huaux, F., Moreau, N., Misson, P., Heilier, J. F., Delos, M., . . . Lison, D. (2005). Respiratory toxicity of multi-wall carbon nanotubes. *Toxicology and Applied Pharmacology*, 207(3), 221–31.

National Institute for Occupational Safety and Health (NIOSH). (2003). *NIOSH manual of analytical methods* (NIOSH Publication No. 2003-154). Washington, D.C.: U.S. Government Printing Office.

National Institute for Occupational Safety and Health (NIOSH). (2005a). *NIOSH pocket guide to chemical hazards* (NIOSH Publication No. 2005-149). Washington, D.C.: U.S. Government Printing Office.

National Institute for Occupational Safety and Health (NIOSH). (2005b). *Current intelligence bulletin: Evaluation of health hazard and recommendations for occupational exposure to titanium dioxide* (NIOSH Docket #100). Washington, D.C.: U.S. Government Printing Office. Retrieved from http://www.cdc.gov/niosh/review /public/tio2/pdfs/TIO2Draft.pdf.

National Institute for Occupational Safety and Health (NIOSH). (2010). *Current Intelligence Bulletin: Occupational exposure to carbon nanotubes and nanofibers* (NIOSH Docket # 161A). Washington, D.C.: U.S. Government Printing Office. Retrieved from http://www.cdc.gov/niosh/docket/review/ docket161A/pdfs/ carbonNanotubeCIB_PublicReviewOfDraft.pdf.

Nel, A., Xia, T., Madler, L., & Li, N. (2006). Toxic potential of materials at the nanolevel. *Science*, 311(5761), 622-627.

Northington, D. J. (1987). Inductively coupled plasma-mass spectrometry for the analysis of metals in membrane filters. *American Industrial Hygiene Association Journal*, 48(12), 977-979.

Oberdörster, G., Ferin, J., & Lenhert, B. E. (1994). Correlation between particle size, in vivo particle persistence, and lung injury. *Environmental Health Perspectives*, 102(suppl. 5), 173-179.

Oberdörster, G., Ferin, J., Gelein, F., Soderholm, S. C., & Finkelstein, J. (1992). Role of the alveolar macrophage in lung injury: Studies with ultrafine particles. *Environmental Health Perspectives*, 97, 193–199.

Oberdörster, G., Sharp, Z., Atudorei, V., Elder, A., Gelein, R., Kreyling, W., & Cox, C. (2004). Translocation of inhaled ultrafine particles to the brain. *Inhalation Toxicology*, 16, 437-445.

Oberdörster, G., Sharp, Z., Atudorei, V., Elder, A., Gelein, R., Lunts, A., . . . Cox, C. (2002). Extrapulmonary translocation of ultrafine carbon particles following whole-body inhalation exposure of rats. *Journal of Toxicology and Environmental Health, Part A*, 65, 1531-1543.

Papp, T., Schiffmann, D., Weiss, D., Castranova, V., Vallyathan V., & Rahman, Q. (2008). Human health implications of nanomaterial exposure. *Nanotoxicology*, 2(1), 9-27.

Park, J. Y., Ramachandran, G., Raynor, P. C., Eberly, L. E., & Olson, G. Jr. (2010). Comparing exposure zones by different exposure metrics using statistical parameters: Contrast and precision. *The Annals of Occupational Hygiene*, 54(7), 799-812. doi:10.1093/annhyg/meq043

Pauluhn, J. (2010). Subchronic 13-week inhalation exposure of rats to multiwalled carbon nanotubes: Toxic effects are determined by density of agglomerate structures, not fibrillar structures. *Toxicological Sciences*, 113(1), 226-242.

Peters, T. M., Elzey, S., Johnson, R., Park, H., Grassian, V. H., Maher, T., & O'Shaughnessy, P. (2009a). Airborne monitoring to distinguish engineered nanomaterials from incidental particles for environmental health and safety. *Journal of Occupational and Environmental Hygiene*, 6(2), 73–81.

Peters, T. M., Heitbrink, W. A., Evans, D. E., Slavin, T. J., & Maynard, A. D. (2006). The mapping of fine and ultrafine particle concentrations in an engine machining and assembly facility. *The Annals of Occupational Hygiene*, 50(3), 249-57.

Peters, T. M., Volckens, J., & Hering, S. V. (2009b). *Impactors, cyclones, and other particle collectors: A monograph of the ACGIH® air sampling instruments* (Committee publication #ASI13). Cincinnati, OH: American Conference of Governmental Industrial Hygienists.

Peters. T. M., & Volkwein, J. C. (2003). Analysis of sampling line bias on respirable mass measurement. *Applied Occupational and Environmental Hygiene*, 18(6), 458–465.

Phillips, J. I., Green, F. Y., Davies, J. C., & Murray, J. (2010). Pulmonary and systemic toxicity following exposure to nickel nanoparticles. *American Journal of Industrial Medicine*, 53, 763-767.

Porter, D. W., Hubbs, A. F., Mercer, R. R., Wu, N., Wolfarth, M. G., Sriram, K., . . . Castranova, V. (2010). Mouse pulmonary dose-and time course-responses induced by exposure to multi-walled carbon nanotubes. *Toxicology*, 269, 136-147.

Ramachandran, G. (2005). *Occupational exposure assessment for air contaminants*. Boca Raton, FL: CRC Press, Taylor & Francis Group.

Rendall, R. E. G., Phillips, J. I., & Renton, K. A. (1994). Death following exposure to fine particulate nickel from a metal arc process. *The Annals of Occupational Hygiene*, 38, 921-930.

Roco, M. C. (2004). Science and technology integration for increased human potential and societal outcomes. *Annals of the New York Academy of Sciences*, 1013, 1-6.

Sandstrom, A. I. M., Wall, S. G. I., & Taube, A. (1989). Cancer incidence and mortality among Swedish smelter workers. *British Journal of Industrial Medicine*, 46, 82-89.

Sargent, L. M., Shvedova, A. A., Hubbs, A. F., Salisbury, J. L., Benkovic, S. A., Kashon, M. L., . . . Reynolds, S. H. (2009). Induction of aneuploidy by single-walled carbon nanotubes. *Enviromental and Molecular Mutagenesis*, 50(8), 708-717.

Schulte, P., Geraci, C., Zumwalde, R., Hoover, M., Castranova, V., Kuempel, E., . . . Savolainen, K. (2008a). Sharpening the focus on occupational safety and health in nanotechnology. *Scandinavian Journal of Work, Environment & Health*, 34(6), 471-478.

Schulte, P., Geraci, C., Zumwalde, R., Hoover, M., & Kuempel, E. (2008b). Occupational risk management of engineered nanoparticles. *Journal of Occupational and Environmental Hygiene*, 5(4), 239-49.

Shvedova, A. A., Castranova, V., Kisin, E., Schwagler-Berry, D., Murray, A. R., Gandelsman, V. Z., . . . Baron, P. (2003). Exposure to carbon nanotube material: Assessment of nanotube cytotoxicity using human keratocyte cells. *Journal of Toxicology and Environmental Health*, *Part A*, 66(20), 1909-1926.

Shvedova, A. A., Kisin, E. R., Mercer, R., Murray, A. R., Johnson, V. J., Potapovich, A. I., . . . Baron, P. (2005). Unusual inflammatory and fibrogenic pulmonary responses to single walled carbon nanotubes in mice. *American Journal of Physiology: Lung Cellular and Molecular Physiology*, 289(5), L698-L708.

Shvedova, A. A., Kisin, E., Murray, A. R., Johnson, V. J., Gorelik, O., Arepalli, S., . . . Kagan, V. (2008). Inhalation vs. aspiration of single-walled carbon nanotubes in C57BL/6 mice: Inflammation, fibrosis, oxidative stress and mutagenesis. *American Journal of Physiology: Lung Cellular and Molecular Physiology*, 295, L552−L565.

Sinclair, D., & Hoopes, G. S. (1975). A novel form of diffusion battery. *American Industrial Hygiene Association Journal*, 36, 39-42.

Soderholm, S. C. (1989). Proposed international conventions for particle size-selective sampling. *Annals of Occupational Hygiene.* 33, 301-320.

Soderholm, S.C., McCawley, M.A. (1990) Should dust samplers mimic human lung deposition? *Applied Occupational and Environmental Hygiene*; 5, 829–35.

Solomon, P. A., Norris, G., Landis, M., & Tolocka, M. (2001). Chemical analysis methods for atmospheric aerosol components. In P. A. Baron & K. Willeke (Eds.), *Aerosol measurement: Principles, techniques, and applications* (2nd ed., pp. 261-293). New York, NY: John Wiley and Sons, Inc.

Stern, S. T., & McNeil, S. E. (2008). Nanotechnology safety concerns revisited. *Toxicological Sciences*, 101(1), 4–21.

Tejral, G., Panyala, N. R., & Havel, J. (2009). Carbon nanotubes: Toxicological impact on human health and environment. *Journal of Applied Biomedicine*, 7, 1-13.

Timonen, K. L., Vanninen, E., de Hartog, J., Ibald-Mulli, A., Brunekreef, B., Gold, D. R., . . . Pekkanen, J. (2005). Effects of ultrafine and fine particulate and gaseous air pollution on cardiac autonomic control in subjects with coronary artery disease: The ULTRA study. *Journal of Exposure Analysis and Environmental Epidemiology*, 16(4), 332-341.

Tolocka, M. P., Tseng, P. T., & Wiener, R. W. (2001). Optimization of the wash-off method for measuring aerosol concentrations. *Aerosol Science and Technology,* 34(5), 416-421.

Tsai, S., Hofmann, M., Hallock, M., Ada, E., Kong, J., & Ellenbecker, M. (2009a). Characterization and evaluation of nanoparticle release during the synthesis of single-walled and multiwalled carbon nanotubes by chemical vapor deposition. *Environmental Science and Technology*, 43, 6017-6023.

Tsai, S., Ada, E., Isaacs, J., & Ellenbecker, M. (2009b). Airborne nanoparticle exposures associated with the manual handling of nanoalumina and nanosilver in fume hoods. *Journal of Nanoparticle Research*, 11(1), 147–161.

Tsuji, J. S., Maynard, A. D., Howard, P. C., James, J. T., Lam, C. W., Warheit, D. B., & Santamaria, A. B. (2006). Research strategies for safety evaluation of nanomaterials, part IV: Risk assessment of nanoparticles. *Toxicological Sciences*, 89(1), 42-50.

Tuchman, D. P., Volkwein, J. C., & Vinson, R. P. (2008). Implementing infrared determination of quartz particulates on novel filters for a prototype dust monitor. *Journal of Environmental Monitoring*, 10, 671–678.

Vanderpool, R. W., Peters, T. M., Natarajan, S., Gemmill, D. B., & Wiener, R. W. (2001). Evaluation of the loading characteristics of the EPA WINS PM2.5 separator. *Aerosol Science and Technology*, 34, 444-456.

Vincent, J. H. (1999). *Particle size-selective sampling for particulate air contaminants*. Cincinnati, OH: American Conference of Governmental Industrial Hygienists (ACGIH).

Vincent, J. H., Mark, D., Miller, B. G., Armbruster, L., & Ogden, T. L. (1990). Aerosol inhalability at higher windspeeds. *Journal of Aerosol Science*, 21, 577-586.

von Klot, S., Peters, A., Aalto, P., Bellander, T., Berglind, N., D'Ippoliti, D., . . . Forastiere, F. (2005). Ambient air pollution is associated with increased risk of hospital cardiac readmissions of myocardial infarction survivors in five European cities. *Circulation*, 112(20), 3073-3079.

Wang, J., Chen, D. R., & Pui, D. Y. H. (2007). Modeling of filtration efficiency of nanoparticles in standard filter media. *Journal of Nanoparticle Research*, 9, 109-115.

Warheit, D. B., Laurence, B. R., Reed, K. L., Roach, D. H., Reynolds, G. A. M., & Webb, T. R. (2003). Comparative pulmonary toxicity assessment of single-wall carbon nanotubes in rats. *Toxicological Sciences*, 77, 117-125.

Wichmann, H., & Peters, A. (2000). Epidemiological evidence of the effects of ultrafine particles exposure. *The Royal Society*, 358, 2751-2769.

Wunder, J. (2000). Quantitative fume hood evaluation for operator safety. *Chemical Health and Safety*, 7(4), 26-30.

Yamamoto, N., Kumagai, K., Fujii, M., Shendell, D. G., Endo, O., & Yanagisawa, Y. (2005). Size-dependent collection of micrometer-sized particles using nylon mesh. *Atmospheric Environment*, 39, 3675-3685.

Yeh, H. C., Cheng, Y. S., & Orman, M. M. (1982). Evaluation of various types of wire screens as diffusion battery cells. *Journal* of *Colloid and Interface Science*, 86(1),12-16.

Yu, M. F., Louire, O., Dyer, M. J., Moloni, K., Kelly, T. F., Ruoff, R. S. (2000). The strength and breaking mechanism of multiwalled carbon nanotubes under tensile load. *Science*, 287, 637-640.

Zhu, Y., Hinds, W. C., Kim, S., & Sioutas, C. (2002). Concentration and size distribution of ultrafine particles near a major highway. *Journal of the Air & Waste Management Association*, 52(9), 1032-42.